ACS Biomaterials SCIENCE & ENGINEERING

pubs.acs.org/journal/abseba Article

Three-Dimensional Printing Using a Maize Protein: Zein-Based Inks in Biomedical Applications

Jorge Alfonso Tavares-Negrete,[#] Alberto Emanuel Aceves-Colin,[#] Delia Cristal Rivera-Flores, Gladys Guadalupe Díaz-Armas, Anne-Sophie Mertgen, Plinio Alejandro Trinidad-Calderón, Jorge Miguel Olmos-Cordero, Elda Graciela Gómez-López, Esther Pérez-Carrillo, Zamantha Judith Escobedo-Avellaneda, Ali Tamayol, Mario Moisés Alvarez,* and Grissel Trujillo-de Santiago*

Cite This: *ACS Biomater. Sci. Eng.* 2021, 7, 3964−3979 Read Online

ACCESS | Metrics & More | Article Recommendations | Supporting Information

ABSTRACT: The use of three-dimensional (3D) printing for biomedical applications has expanded exponentially in recent years. However, the current portfolio of 3D printable inks is still limited. For instance, only few protein matrices have been explored as printing/bioprinting materials. Here, we introduce the use of zein, the primary constitutive protein in maize seeds, as a 3D printable material. Zein-based inks were prepared by dissolving commercial zein powder in ethanol with or without polyethylene glycol (PEG400) as a plasticizer. The rheological characteristics of our materials, studied during 21 days of aging/maturation, showed an increase in the apparent viscosity as a function of time in all formulations. The addition of PEG400 decreased the apparent viscosity. Inks with and without PEG400 and at different maturation times were tested for printability in a BioX bioprinter. We optimized the 3D printing parameters for each ink formulation in terms of extrusion pressure and linear printing velocity. Higher fidelity structures were obtained with inks that had maturation times of 10 to 14 days. We present different proof-of-concept experiments to demonstrate the versatility of the engineered zein inks for diverse biomedical applications. These include printing of complex and/or free-standing 3D structures, tablets for controlled drug release, and scaffolds for cell culture.

KEYWORDS: *3D printing, zein, corn grain, biofabrication, drug release, cell culture*

1. INTRODUCTION

Engineers and scientists are actively seeking to harness the advantages of three-dimensional (3D) printing to provide improved solutions to current challenges associated with bioengineering (*i.e.*, the development of tissues and organs,[1] the smart design of implants[2] or wearables for real-time physiological monitoring,[3] the production of cultured meat,[4] and the engineering of ecofriendly, and cost-effective products,[5] among others). The advantages of traditional extrusion-based 3D printing include layer-by-layer fabrication of almost any 3D form at relatively high resolution, down to the microscale.[6] For instance, 3D printing has enabled the fabrication of free-form products, such as personalized dosed pills, temporary stents, tissue-engineered heart valves, or full-sized bladders.[7−11] However, the diversity of biomedical devices that can be 3D printed is severely limited by the present portfolio of available printable materials or inks[5,12−14] capable of satisfying the demanding requirements of biomedical applications. Printing will be further enabled by expanding the spectrum of extrudable and biofriendly materials (*i.e.*, biocompatible, resorbable, amenable to biological functionalization, *etc.*).[15,16] Some materials frequently used as inks in extrusion 3D bioprinting are biocompatible and even safe to eat (collagen, gelatin, silk, alginate, agarose, and glycosaminoglycans, among others).[17] In addition to these, several food-based matrices have been explored recently for use in extrusion 3D printing.[18,19] Some examples are carbohydrate-rich foods (*e.g.*, baking dough,[20] glucose and sucrose,[21] starch,[22] cellulose,[23] lignin,[23,24] and plant-based powders[25−27]), fat-rich materials (such as chocolate[28,29]), and protein-rich foods (*e.g.*, milk protein,[30,31] meat,[32] insect powder,[33] cheese,[34] egg protein,[27,35] and vegetable proteins[36]). In the near future, some of these materials could be engineered (in terms of rheology, stability, biocompatibility, *etc.*) for use in the biomedical field.

Received: April 22, 2021
Accepted: June 17, 2021
Published: July 1, 2021

https://doi.org/10.1021/acsbiomaterials.1c00544
ACS Biomater. Sci. Eng. 2021, 7, 3964−3979

Among the many possibilities, protein-based materials are particularly attractive. Proteins are constitutive blocks in the human body; therefore, their use may lead to the design of biocompatible, resorbable, cell-friendly, and biosmart inks for biomedical applications. Today, only a limited number of protein matrices have been explored as printing/bioprinting materials.[16] Relevant examples are mammal-derived proteins, such as collagen,[37] fibrin,[38] or gelatin.[39] Some of these materials (*i.e.*, collagen and gelatin) are extensively used in bioprinting applications because of their cell-adhesive and bioactive properties that allow cell attachment or interaction. Their mechanical properties are also similar to those of natural tissues, making them suitable host environments for cultured cells.[39−41] However, these proteins have limited availability and typically lack the physical stability needed for 3D printing of precise and large structures (centimeter range).[16] Furthermore, their use often requires tight control over the processing and printing temperature, chemical prefunctionalization such as methacrylation, and postprinting cross-linking steps.[42−44] These processability challenges are further complicated by the limited availability of mammal-derived materials and, thus, their high cost.[16,39,45]

Fortunately, alternative 3D printing materials can be found outside the mammal group. For instance, silks from arthropods and insects exhibit excellent characteristics of biocompatibility and stability under physiological conditions and have been confirmed as 3D printable, thereby greatly enhancing their potential in biofabrication.[46] In the present study, we explore the use of zein, the most abundant constitutive protein in maize seeds, as a suitable material for developing 3D printing materials. Zein, as a byproduct of corn syrup or cornstarch production, is a widely abundant and cost-effective plant-derived biopolymer.[47,48] It is a prolamine, a protein rich in the amino acid proline, and occurs as aggregates linked by disulfide bonds.[49,50] It has a molecular weight around 25,000 to 35,000 kDa and is poorly soluble in water due to its relatively high content of hydrophobic amino acids (proline, leucine, and alanine); however, it also exhibits amphiphilic behavior due to its high glutamine content (21−26%).[47,51]

Here, we explore the use of concentrated zein solutions in ethanol/water as inks for 3D printing, aiming to expand the portfolio of proteins used in 3D printing. Zein exhibits several attractive attributes as a printable material. Zein is biodegradable, edible, has been classified as "generally recognized as safe" by the U.S. Food and Drug Administration (FDA),[52] and has been used in biomedical applications, such as coatings for pharmaceutical capsules,[47,48,51] fabrication of scaffolds for cell culture,[53] and synthesis of nanoparticles,[54] fibers,[55] and membranes[56] for controlled drug release.

Zein and poly ε-caprolactone blends[57,58] and zein−lignin blends[24] have also been used before in 3D printing applications. Furthermore, previous studies have shown that concentrated zein solutions in ethanol/water exhibit shear-thinning properties,[59] a required characteristic of inks used for extrusion-based 3D printing. To our knowledge, this is the first report of the use of zein as a 3D printing material.

Zein-based formulations, optionally supplemented with polyethylene glycol (PEG400) as a plasticizer,[53,60] were characterized in terms of their rheology, printability, and stability. We also report the effect of ink aging time on the rheological properties and printability. The shape fidelity and self-standing behavior of zein-based inks was successfully demonstrated by the 3D printing of complex multilayer constructs. Furthermore, we show proof-of-concept experiments that demonstrate potential applications of our formulations. For instance, we 3D printed zein (Z) and zein−PEG (ZP) antibiotic-loaded tablets and studied their release kinetics and bacterial inhibition properties. Moreover, 3D printed zein scaffolds were seeded with C2C12 myoblasts to assess cytocompatibility.

2. MATERIALS AND METHODS

2.1. Materials. Zein (Z3625, SLBV3020), poly-(ethylene glycol) 400 (P3265, MKBG3641V), Dulbecco's modified Eagle's medium (DMEM; D5748, SLBW4140), Dulbecco's phosphate buffered saline (PBS; D5773, SLBW277), nalidixic acid (NA; N8878, BCBW6556), and 4′,6-diamidino-2-phenylindole (DAPI; D9542, 28718-90-3) were purchased from Sigma-Aldrich, USA. Mouse myoblast cells (C2C12, ATCC CRL-1772) and *Staphylococcus aureus* (ATCC 29213) were purchased from American Type Culture Collection (ATCC), USA. Fetal bovine serum (FBS, 16000-044, 2087367) and antibiotic−antimycotic 100× (15240062) were purchased from Gibco (Grand Island, USA). Phalloidin-iFluor 647 (ab176759, GR3256003-6) was purchased from Abcam. PrestoBlue (A13261, 2044809) was purchased from Invitrogen. Luria−Bertani broth medium was purchased from Difco, MD, USA.

2.2. Zein Ink Preparation. We prepared two different zein ink formulations (Figure 1). A pristine zein ink (Z) was prepared by solubilizing 15 g of zein in 20 mL of 70% ethanol aqueous solution. This mixture was homogenized by vortexing for 10 to 15 min, then heated at 45 °C for 20 min under manual and gentle agitation, and then stored (when still hot) in tightly closed sterile 10 mL syringes to avoid further solvent evaporation and water uptake. Inks were maintained at room temperature (~25 °C) until use.

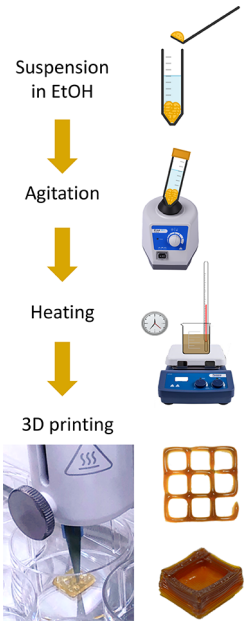

Figure 1. Preparation and characterization of zein inks for 3D printing. Schematic representation of the protocol for preparation of zein-based inks. Zein powder was added to an aqueous ethanol solution and gradually incorporated by vortexing to generate a suspension, which was subsequently heated to produce a homogeneous solution. These formulations were placed in tightly closed syringes and stored for up to 21 days. See Videos S1 and S2.

The zein−PEG ink (ZP) was prepared using the described protocol and additionally incorporating 2 g of PEG400 into the mix of 15 g zein in 20 mL of 70% v/v of ethanol aqueous solution. The PEG400 was added during the first 10 min of heating. The rheological and

https://doi.org/10.1021/acsbiomaterials.1c00544
ACS Biomater. Sci. Eng. 2021, 7, 3964−3979

printability characterization of these inks was conducted after 1, 7, 10, 14, and 21 days of storage/aging time.

2.3. Rheological Characterization of Zein Inks. The rheology of the zein inks was evaluated using a MCR 500 rheometer (Anton Paar Rheoplus, Austria) equipped with a Peltier device for temperature control. A 50 mm parallel plate geometry and a gap of 5 mm were used for all measurements. In the first set of experiments, the effective viscosity, the storage modulus (G'), and the loss modulus (G'') were measured using an angular frequency of 10 rad s^{-1} and a shear rate between 0 and 0.5 s^{-1} at room temperature at different aging/maturation times (0 and 21 days). Three independent repeats were performed (n = 3).

We calculated yield stresses for our zein inks from the modulus versus shear stress data. Yield stresses were calculated as the first point of shear stress (pressure) at which the value of G' decreases at least 5% in a sustained manner along the trajectory of increasing values of shear (see also Figure S3). We also calculated the flow point, which is the point of crossing between the storage (G') and the loss modulus (G'') in the modulus versus shear stress plot.

In addition, a temperature sweep was conducted to characterize the temperature dependence of the rheological properties of the Z and ZP formulations. In this experiment, the viscosity of zein was measured with a temperature ramping from 48 to 8 °C at a cooling rate of 1 °C/min and a constant shear rate of 1 s^{-1}.

2.4. Printability Studies. We evaluated the printability of zein-based formulations by printing a grid design at different combinations of relevant printing variables, including extrusion pressure, printing velocity, and ink maturation time. Three settings of pressure (65, 75, and 85 kPa), printing velocity (3, 5, and 7 mm/s), and ink maturation times (4, 7, 10, and 14 days) were explored in our printing experiments. These ranges of values for pressure and linear speed were selected based on preliminary experiments. All 3D printing experiments were conducted using a BioX (CELLINK, Sweden) bioprinter. Cartridges (3 mL volume) were filled with Z and ZP inks aged for 4, 7, 10, or 14 days. Blue high-precision conical 22 G nozzles (410 μm internal diameter) from CELLINK were used for printing. Four-layer reticles (grids) of 2 × 2 cm were extruded at room temperature (~25 °C). In the case of our zein inks, deformations can certainly occur (especially with those inks that are more fluid). For these characterizations, we took pictures of the grids immediately after printing.

We also evaluated the effect of the extrusion temperature (at the nozzle) on the printability of zein-based inks. To do this, we fabricated grids of Z and ZP formulations at temperatures of 10, 25, and 45 °C using a pressure setting of 75 kPa and a linear printing velocity of 3 mm/s.

2.5. Characterization of the Fidelity of the Printed Structures. We evaluated the fidelity of grid structures printed with zein-based inks using image analysis techniques. Photographic images of printed structures were analyzed using ImageJ 1.52q software. The heights and widths of the empty spaces between each zein line were measured by transforming the photographs into 8 bit images and modifying their contrast to facilitate the detection of borders. In general, a set of 18 lines for each group was obtained and averaged. The inner square length (ISL) values were reported in the main text of this work only for grids that (a) contained at least 12 measurable lines and (b) did not exhibit clumps.

The average ISL values were graphed with their corresponding standard deviations. At least six evaluations of the ISL value (n = 6) were performed per grid.

2.6. Compressive Mechanical Testing. We studied the compressive properties of printed cylinders fabricated with Z and ZP in compressive tests using a Stable Micro Systems texture analyzer (TA-XT plus, Stable Micro Systems Ltd., UK). We fabricated small cylinders (10 mm in diameter) of Z and ZP in our bioprinter, let them dry for 7 days, and obtained stress versus deformation curves. We conducted 5 and 6 independent repeats of the compressive test for Z and ZP cylinders, respectively (N = 5, 6). In these experiments, we used a compressive speed of 1.33 mm/s.

2.7. Fourier Transform Infrared Spectroscopy Analysis. Fourier-transform infrared (FTIR) spectroscopy analysis was performed to evaluate the effect of aging and water exposure on the protein secondary structures of zein-based inks.

The FTIR spectra of 7 and 14 day aged Z and ZP inks, before and after immersion in water, were obtained using a FTIR/FT-NIR PerkinElmer Spectrum 400, equipped with a total attenuated reflection (ATR) accessory. Sixteen scans per sample at 4 cm^{-1} resolution were acquired over the range of 1100−1900 cm^{-1}. A secondary-structure analysis was performed by band-narrowing techniques, second-derivative analysis, and Fourier self-deconvolution using the Origin software (version 2019). In particular, the spectral region from 1570 to 1720 cm^{-1}, corresponding to the amide I region, was analyzed following the protocol described by Yang *et al.*[61] The bands with a frequency of 1650−1658 cm^{-1} were assigned to α-helixes, from 1640 to 1650 cm^{-1} to nonordered structures or random coils, from 1660 to 1680 cm^{-1} to loop or β-turns, and from 1620 to 1640 and 1670−1695 cm^{-1} to β-sheets.[61]

2.8. Construct Stability under Aqueous Conditions. We also evaluated the stability of 3D printed zein grids in culture medium. In brief, we incubated grids in DMEM cell culture medium at 37 °C. The thicknesses of the lines of the grids printed using Z and ZP inks were measured over a period of 7 days of incubation using brightfield microscopy. The integrity of the construct (n = 6) was calculated according to the following equation

$$\text{Construct integrity (\%)} = \frac{\text{measured thickness}}{\text{initial thickness}} \times 100$$

We also explored the behavior of the zein-based printed constructs following exposure to different aqueous environment scenarios. For this purpose, we printed spiral structures at 50 kPa and 7 mm/s in a six-well plate (one spiral per well) using a Z and ZP inks with 7 days of maturation. In a first set of experiments, we fully covered the freshly printed spirals (adhered to the well surface) with 5 mL of distilled water at 25 °C for 30 min immediately after printing. In the second set of experiments, the zein spirals were desiccated for 48 h after printing to remove the ethanol. The spirals spontaneously detached from the well surfaces during the desiccation process. The structures were then submerged in water at 25 °C for 30 min. All structures were photographed immediately after recovery from the water bath. This experiment was conducted with three technical repeats (n = 3). The printing conditions for this experiment were 50 kPa, 7 mm/s, not 50 kPa, 20 mm/s. This particular experiment was made with "young" zein ink (7 days of maturation). Therefore, we used a lower pressure than in the experiments depicted in Figure 3.

2.9. Drug Release Studies. We evaluated the release of an antibiotic from 3D printed Z and ZP tablets loaded with NA. In brief, a solution of 45 mg of NA in 40 mL of 70% ethanol was used to prepare these zein inks. Except the addition of NA to the ethanol solution, the Z and ZP inks were prepared as described previously while maintaining temperatures at 37 °C during dissolution to preserve the NA antibiotic activity. Homogeneous solutions containing 3 mg of NA per gram zein were obtained by vortexing. Cylindrical tablets 5.6 mm in height and 10 mm in diameter were printed using the BioX printer and dried in a desiccator for 3 days. The printed tablets of Z and ZP were placed in 15 mL Falcon tubes containing 10 mL of PBS and left to float freely at 37 °C and pH = 7 in a water bath to study drug-release kinetics under physiological conditions. Throughout the drug release experiments, 1 mL aliquots of PBS were withdrawn for analysis and fresh PBS was added to maintain a constant volume. The release of NA into the medium was determined by measuring absorbance at 258 nm using a NanoDrop 1000 spectrophotometer (Thermo Fisher Scientific, USA). We used a calibration curve to correlate the absorbance with NA concentrations in the range of 0.5 to 500 $\mu g\ \mu L^{-1}$. Three independent experiments (N = 3) were conducted with three technical repeats (n = 3).

2.10. Antibiograms. We performed assays to evaluate the antimicrobial activity of NA released from 3D printed zein tablets on *S. aureus* strains. The bacteria were cultured in tryptic soy broth overnight at 37 °C under continuous shaking until the optical density

https://doi.org/10.1021/acsbiomaterials.1c00544
ACS Biomater. Sci. Eng. 2021, 7, 3964−3979

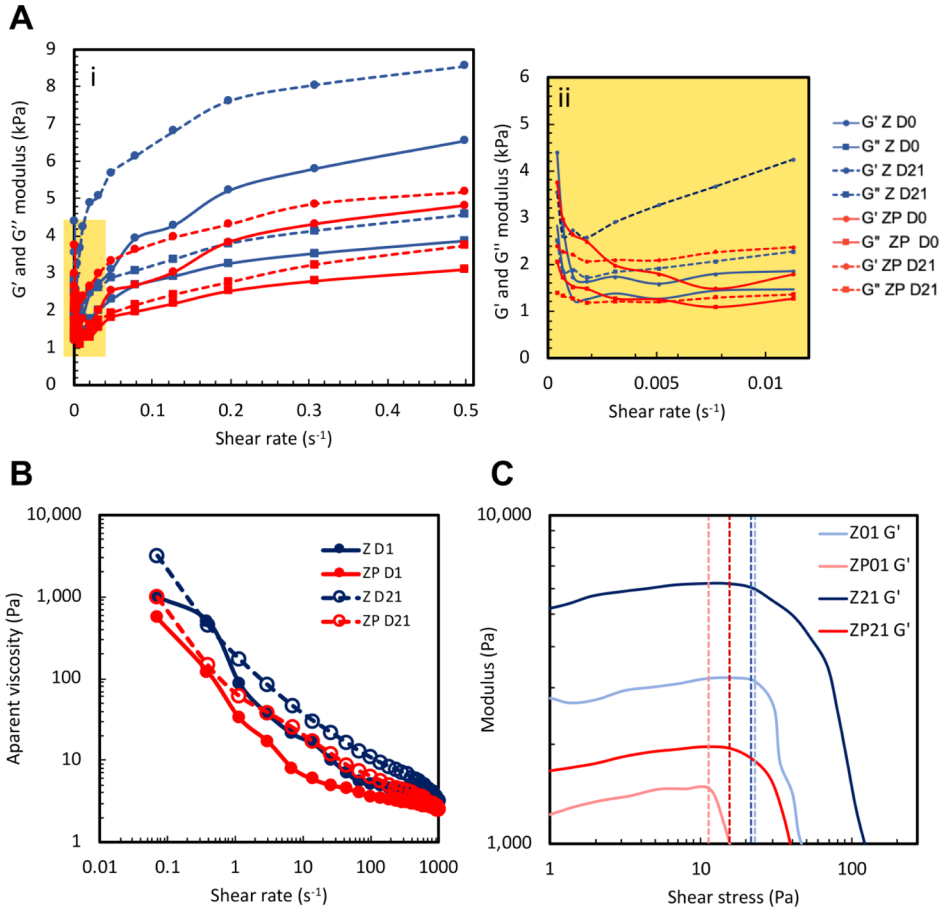

Figure 2. Rheological characterization of zein (Z) and zein + PEG400 (ZP) inks was conducted at day 0 and 21: (A) storage (G') and loss modulus (G'') and (B) apparent viscosity of zein formulations at room temperature as a function of the shear rate (n = 3). (C) Shear stress *vs* storage modulus for different Z and ZP inks (aged at day 1 or 21) as calculated at room temperature. The yield points (or yield stresses), calculated from a graphic analysis, are indicated with vertical lines.

reached 0.6−0.8 (at 600 nm).[62,63] Tablet dissolution methods were used to determine the antimicrobial effect of 3D printed discs according to antimicrobial testing guidelines.[64] In brief, for broth dilution experiments, 1 mL of Mueller−Hinton broth was placed in Falcon tubes and 100 μL of bacterial suspension was added. The 3D printed tablets of different zein formulations (*i.e.*, Z, ZP, Z-nalidixic, and ZP-nalidixic) were then placed into the tubes. Tubes were shaken at 100 rpm and 37 °C for 48 h until the final reading at 600 nm. Tests were performed in triplicate (n = 3).

In addition, we conducted convectional antibiograms in Petri dishes. In brief, bacterial dilutions containing 10^7 colony forming units (c.f.u.) of *S. aureus* were plated in solid plate count agar and incubated at 37 °C in the presence of 3D printed cylindrical zein tablets (of 5.6 mm in height and 10 mm in diameter). Each tablet contained ∼1.32 mg NA. The area and diameter of the inhibition halo was measured 72 h after seeding using image analysis techniques. Tests were performed in triplicate (n = 3).

2.11. Cell Scaffolding. We conducted cell culture experiments using 3D printed grids of 2 × 2 cm with Z and ZP inks as cellular scaffolds. We extruded two-layer grids (0.81 mm height) with a BioX 3D bioprinter and dried the grids in a desiccator for 7 days to evaporate the ethanol used to prepare the inks. The grids were sterilized under UV light overnight and then placed in six-well ultralow attachment plates and washed 3 times with PBS to remove residual ethanol. FTIR analysis was conducted to determine the ethanol content in the washing supernatant. In brief, a PerkinElmer FTIR/ATR Spectrum 400 NIR/mid-IR spectrophotometer was used to detect the ethanol peak at 2991 cm^{-1} in the PBS washing supernatant from dried (7 days in a desiccator) Z and ZP samples. The spectra of supernatant drops were recorded in the range of 4000−400 cm^{-1} at a resolution of 4 cm^{-1} and 16 scans per sample (n = 3).

In the first round of cell-culture experiments, grids were surface-seeded with C2C12 myoblast cells (ATCC CRL 1772) by covering the grids with a C2C12 cell suspension containing 5 × 10^5 cells mL^{-1} and incubating for 24 h at 37 °C to promote attachment. Nonattached cells were removed after this incubation period. We ran parallel cell culture experiments in conventional six-well plates as a control. The cultures were maintained in 3 mL of DMEM culture medium supplemented with 10% FBS and 1% antibiotic−antimycotic and incubated at 37 °C in a 5% CO_2 atmosphere for 7 days. The grids were observed at days 0, 1, 3, and 7 using an Axio M2 Observer fluorescence microscope (ZEISS, Germany). PrestoBlue metabolic activity assays were performed at day 0, 1, 3, and 7. The samples at day 7 were stained with phalloidin (1:1000 in PBS) and DAPI (1:1000 in PBS) at 4 °C overnight, washed 3 times with PBS, and observed under the fluorescence microscope. Two independent experiments (N = 2) with triplicates (n = 3) were conducted.

In the second round of cell culture experiments, 3D printed Z and ZP grid scaffolds were incubated in 50 mg mL^{-1} fibronectin in PBS overnight at 4 °C to enhance cellular attachment. After incubation, the fibronectin solution was removed and the grids were placed in fresh ultra-low adhesion well plates. C2C12 cells were seeded over the grids and cultured for 7 days, as described before. Cell attachment and spreading were observed by fluorescence imaging with phalloidin and DAPI staining on day 7. All experiments were conducted in triplicate (n = 3).

2.12. Scanning Electron Microscopy. We analyzed the internal microstructure of the different zein ink formulations using scanning electron microscopy (SEM). A line of zein ink was extruded using a

https://doi.org/10.1021/acsbiomaterials.1c00544
ACS Biomater. Sci. Eng. 2021, 7, 3964−3979

syringe and subsequently stored in a desiccator for 7 days at room temperature. Cross sections of the dried constructs printed with zein inks aged for 7, 14, and 21 days were exposed by manual breaking. These cross sections were coated with gold using a Q150R ES rotating sputter machine (Quorum, United Kingdom) prior to imaging. SEM micrographs were obtained at 500× magnification in a ZEISS EVO MA25 SEM (Germany). Three technical repeats (n = 3) and three images per sample were analyzed.

The number and projected area of the zein pores were measured using ImageJ from the SEM images. Results were analyzed in MATLAB R2018B to evaluate the evolution of pore size distribution through aging in zein formulations with or without PEG400. The pore size values were grouped in 12 bins spanning the range from 0.20 to 15.32 μm^2. We reported pore size distributions and cumulative frequency plots based on these calculations.

2.13. Statistical Analysis. Analysis of variance was performed with Minitab Express 1.5 (2017). Differences with a p value <0.05 (*) were considered statistically significant.

3. RESULTS AND DISCUSSION

Here, we introduced the use of zein, the primary constitutive protein in maize, as a 3D printable material. Two different ink formulations were prepared by dissolving commercial zein powder in ethanol (Z) and optionally adding PEG400 as a plasticizer (ZP).

The selection of PEG400 as a plasticizer was based on our previous experience and reports from colleagues. PEG400 has been formally studied and is well described as a good plasticizer for zein and zein blends.[65] In preliminary assays, we learned that using the same PEG concentration as in our previous work (25% dry basis; blend of zein powder and PEG400) results in inks with very low viscosity. Therefore, for this work, we decided to use half the concentration that we used in our previous reports.[53,66]

Figure 1 schematically shows the method of preparation of these zein inks. In brief, zein powder was dispersed in ethanol by vigorous vortexing. The resulting suspension was heated at 45 °C until a homogeneous solution was obtained. For our ZP formulations, PEG400 was added during the first 10 min of heating. Z and ZP formulations were characterized in terms of rheology and printability.

One of the main findings of our work is that the rheological properties of these zein formulations, which dictate their printability attributes, evolve with aging time. We characterized the evolution of these properties (*i.e.*, viscosity, viscoelastic behavior, and printability itself).

3.1. Rheology Characterization. In extrusion printing, the rheology of an ink greatly determines printability.[67−69] We have conducted a detailed rheological characterization of our zein ink formulations at the time of preparation and after 21 days of aging. The following observations were derived from this characterization.

Both zein formulations (Z and ZP) behave as pseudoplastics with $G' \gg G''$ (Figure 2A(i,ii)). This pseudoplastic behavior is maintained over the maturation time of 21 days. Consistently, the storage modulus (G') is higher than the loss modulus (G'') over the whole frequency range, indicating a typical gel behavior.[70] Frequency oscillation experiments showed that the storage (G') and loss modulus values (G'') increased as the Z and ZP ink matured over 21 days. For example, the storage modulus for Z formulations increased from 6.55 ± 0.14 kPa at day 0 to 8.55 ± 0.09 kPa at day 21 when evaluated at the highest shear rate. For ZP formulations, the storage modulus at the highest shear rate increased from 4.82 ± 0.12 kPa at day 0 to 5.18 ± 0.07 kPa at day 21.

Our inks behave as shear thinning materials, meaning that their effective viscosity decreases with increasing shear rates. Remarkably, the viscosity of our zein inks decreases by more than 1 order of magnitude within the window of shear rates that we analyzed (Figure 2B). Overall, shear thinning behavior is a key characteristic sought in inks for extrusion 3D printing[71,72] as it strongly impacts printability. In practical terms, shear thinning inks will exhibit less resistance to flow as more mechanical (or hydraulic) pressure is applied during extrusion. The incorporation of PEG does not alter the shear-thinning behavior of zein inks. As expected, PEG addition yields inks with a lower viscosity and a lower storage modulus.[73] The addition of PEG decreases viscosity, but the slope of the plot of viscosity versus the shear rate does not change (Figure 2B).

We performed additional rheology experiments to calculate yield stresses for our zein inks from the modulus versus shear stress data (Figures 2C and S3; Table S2).

Yield stresses are often used to predict the lower threshold of pressure to achieve adequate printability.[74,75] We also calculated the flow point (Figure S3 and Table S2), which is the point of crossing between the storage (G') and the loss modulus (G''), as this value is also considered a useful predictor of the pressures needed to achieve adequate printability.[74] In our experiments, the yield stress value of ZP was higher than that of Z, which is counterintuitive to us based on our previous rheological assessment (*i.e.*, the addition of PEG400 decreases the effective viscosity of zein-based inks). The values of the flow point, cross-point between G' or G'', are more consistent with our observations, and they indicate that lower pressures are needed for ZP printing than for Z printing.

Note that the viscosity of zein inks is highly dependent on maturation time, and PEG attenuates this effect. For example, at shear rate values in the neighborhood of 0.01 s^{-1}, the viscosity of Z inks increases by approximately 1 kPa with respect to the value on the day of preparation. However, ZP inks exhibit a much lower increment of viscosity (∼0.3 kPa) after 21 days of storage.

The aging effect in zein solutions has been attributed to structural changes in the protein.[59,76] For instance, the aging effect has been related to changes in the secondary structure over time, as analyzed by small-angle X-ray diffraction.[77] A full mechanistic understanding underlying the changes in viscosity in zein inks through aging is beyond the scope of this work; however, we conducted basic FTIR spectroscopy analysis to identify possible structural variations in zein formulations through aging based on the vibrational amide I bands related to the protein secondary structures.[78] We estimated the changing percentages of different structural configurations (*i.e.*, α-helix, β-sheets, β-turns, and nonordered structures or random coils) in the overall structure of zein formulations with aging. The percentage of each secondary structure is available as the Supporting Information (Figure S1 and Table S1). The results suggested that the α-helix content of the Z formulation increased by 2.06% as aging progressed (Table S1). By contrast, the proportion of β-sheets and nonordered structures increased in the aged ZP formulation by 13.34 and 21.08%, respectively, while the percentage of α-helix decreased by 7.69%. During aging, the Z and ZP formulations show a decrease in the content of loop structures (−5.27% for Z and −26.73% for ZP) and an increase in nonordered structures

https://doi.org/10.1021/acsbiomaterials.1c00544
ACS Biomater. Sci. Eng. 2021, 7, 3964−3979

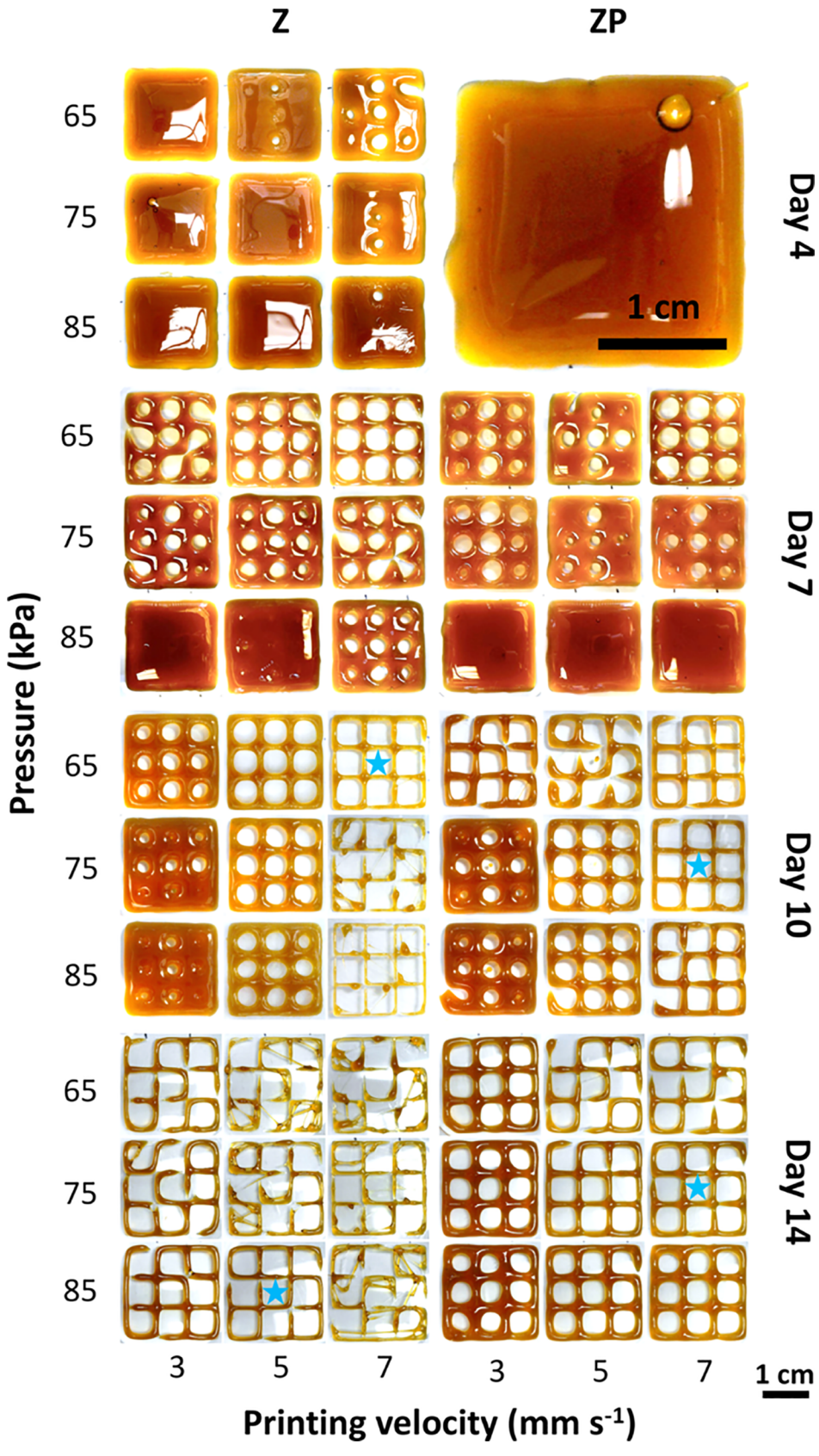

Figure 3. Effect of maturation time on the printability of Z and ZP inks. Different maturation times (*i.e.*, 4, 7, 10, and 14 days), linear printing velocities (*i.e.*, 3, 5, and 7 mm/s), and extrusion pressures (*i.e.*, 65, 75, and 85 kPa) were explored (n = 3). Scale bar: 1 cm. All printings were conducted at room temperature (~25 °C). Blue stars highlight the best printings.

https://doi.org/10.1021/acsbiomaterials.1c00544
ACS Biomater. Sci. Eng. 2021, 7, 3964−3979

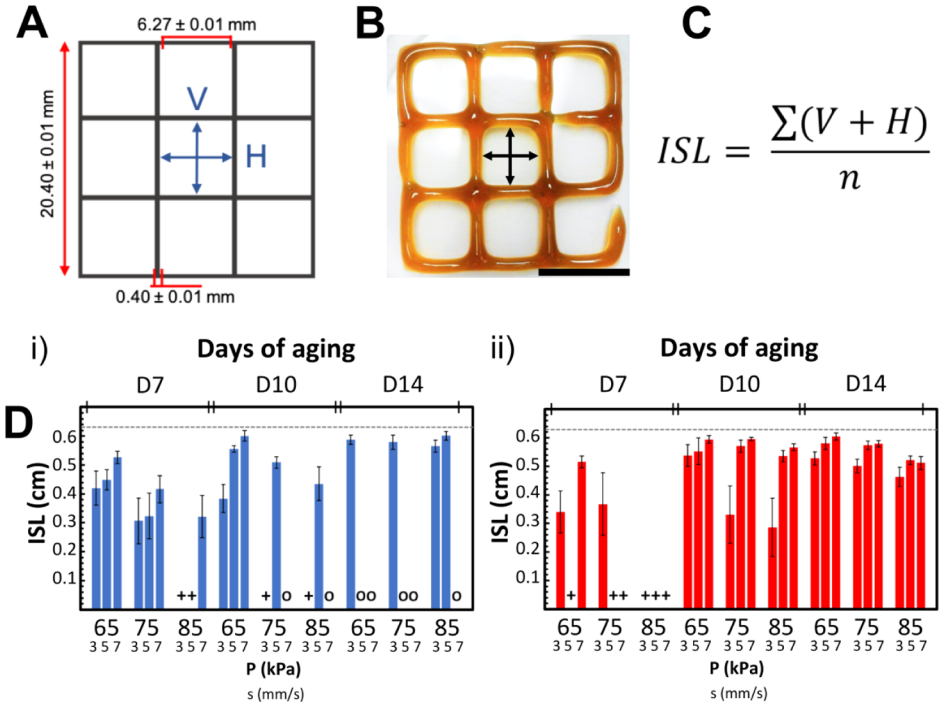

Figure 4. Analysis of the fidelity and quality of our printed zein structures. (A) STL grid design. The theoretical dimensions of vertical (V) and horizontal (H) lines are shown (*i.e.*, V and H = 0.627 cm). (B) Actual printed grid; vertical and horizontal lines are indicated. Scale bar: 1 cm. (C) Equation used to calculate the ISL. (D) ISL values as determined for different printing conditions. Grids printed with zein (Z) and zein−PEG formulations (ZP) were analyzed. ISL values for (i) Z (blue bars), and (ii) ZP (red bars) grids printed at different pressure and speed conditions. Each triplet of bars shows variations depending on linear speed. Analysis is conducted for inks aged 7 (D7), 10 (D10), and 14 (D14) days. Cases in which printing parameters were inadequate to generate continuous and defined structures are marked with a circle (o). When the linear velocity of the printing head was too slow, or the pressure was higher than needed, a cross (+) was assigned. ISL values for all the pressure and linear speed tested are reported in Table S3.

(5.22% for Z and 21.08% for ZP). These observations suggest that the change in viscosity may be induced by changes in the protein structure during aging and that the rate and thermodynamics of these changes might be modified by PEG addition.[59,77]

3.2. Printability of Zein Formulations. Our formulations were printable in a wide range of conditions in a commercially available 3D bioprinter. Printability, or the ability of an ink to be extruded in a manner that creates well-defined structures, is commonly evaluated in terms of the morphology, shape fidelity, and self-standing ability of printed constructs.[79] We evaluated the printability of Z and ZP formulations using a grid design printed with inks at different maturation times. In addition, a matrix of conditions that included different extrusion pressures and printing-head linear velocities was explored. The effect of printing parameters such as applied pressure and print speed on the print fidelity has been studied in detail in recent publications.[80,81]

Figure 3 shows that aging time played a crucial role in the printability of our inks. Freshly prepared Z and ZP inks (at 4 days of aging) were poorly printable under all tested conditions. Their viscosity was too low to render defined grids; instead, a high amount of extruded material formed squared puddles. Low viscosity, as determined at the early stages of maturation, correlates well with the low fidelity of printings conducted using 4 and 7 day aged inks. The higher viscosities of the 10 and 14 day aged inks resulted in improved fidelity. As aging time and viscosity increased, grids with higher definition were obtained (Figures 2 and 3).

The results also showed a clear interplay between ink rheology and printing conditions (linear speed and pressure). Since matured inks (aged >14 days) were more viscous, they required higher pressures and lower velocities to achieve good printability. A clear effect of the plasticizer (PEG400) was also evident in our inks. The incorporation of PEG400 as the plasticizer into zein formulations has been reported before, and this effect was expected.[53,82]

In general, the addition of PEG decreases the viscosity of the ink and enables adequate printing at lower pressures and higher speeds. ZP also extends the time period at which inks can be used and still obtain adequate results. For instance, ZP inks exhibit better printability than Z inks after 14 days of aging. After 14 days of maturation, ZP developed coherent structures at most conditions of pressure and speed. By contrast, Z inks are printable after 14 days of aging only at high pressures. Overall, the window of values of pressures (between 65 and 85 kPa) and printing speed (3 to 7 mm/s) that we used in the experiments described in Figure 3 results in inks that exhibit a wide variety of printing behaviors. We also found that aging had an effect on printability. Of note, none of the 21 day-old inks were printable (*i.e.*, they were very viscous) following the use of this set of pressures and printing speeds.

We conducted a simple quantitative analysis of the quality and fidelity of our printed structures. This analysis was based on the measurement of the distance between opposite parallel lines in printed grids (Figure 4A,B) and comparing the average of these distances among different printing conditions.

The average of these distances, referred to as the inner square length (ISL), is an indicator of fidelity (Figure 4C). ISL

https://doi.org/10.1021/acsbiomaterials.1c00544
ACS Biomater. Sci. Eng. 2021, 7, 3964−3979

analysis offers a more objective view of the influence of printing parameters on printing quality in a real multivariable scenario. Ideally, a single extruded line should be as thick as the nozzle gauge from which it was printed. Therefore, deviations from the designed ISL value are an indicator of deviations from ideal printing quality. For instance, in our experiments, the space between each parallel line in the STL file is 6.27 mm, considering a line thickness of 0.4 mm (diameter of the nozzle outlet) (Figure 4A). In a high-fidelity printing process, the measured ISL should be equal to 6.27 mm, in perfect agreement with the STL design of our grids (Figure 4A).

For a particular printing condition, the standard deviation (STD) of the ISL value relates to reproducibility. Smaller values of STD indicate higher reproducibility. The printing quality among different printing parameters can be evaluated by comparing the measured ISL with the target (*i.e.*, intended ISL) value of 6.27 mm. Figure 4D summarizes the results obtained from this quantitative ISL analysis. Within this set of results, general trends of printing quality, as related to the printing parameters, are readily evident. For instance, Figure 4D clearly shows that, for a particular formulation, fidelity tends to increase with aging. Note that discontinuous structures or cuts in the printed structures were observed under several printing conditions. These printing discontinuities can be attributed to the interplay of rheological and printing parameters. Note that discontinuous structures or cuts in the printed structures were observed under several printing conditions. This occurs when the linear speed of the printhead is higher or the applied pressure is lower than needed for the continuous deposition of the ink (indicated with [o] in Figure 4D(i,ii)). Clumping was also observed for some combinations of parameters. Clumping indicates that the linear velocity of the printhead was lower or the pressure was higher than needed (indicated in Figure 4D(i,ii) with [+]).

In some cases, the ISL of the printed grid is higher than the ideal value. This happens mainly because some layers are printed thinner than the nozzle diameter due to a printing speed that is faster than the flow of the material. The ISL value increases when the filaments are thin (*i.e.*, the numerator of the equation increases). Printed filaments that are thinner than intended (based on the STL file and the nozzle diameter) generate ISL values that are higher than the ideal value. This strategy to produce thin lines has been exploited in the contribution to enhance resolution.[80]

Our printing quality assessment identified a set of additional observations. Printability is evidently a strong function of pressure (see also Figure 2C), and an adequate selection of the pressure setting is key for zein 3D printing. However, the pressure range for feasible printing is wider than that of the speed range. In other words, our results suggest that the printing speed for zein can affect the deposition of the material in a more sensitive way than is observed for pressure. In general, at constant pressure values, the higher the printing speed (within the range of speeds tested), the better the grid fidelity achieved (Figure 4D(i,ii)).

In addition, aging increases viscosity, and higher viscosities ease the control required to achieve high printing quality. Note, however, that the effect of aging in printability is more evident in pristine zein inks than in those with added PEG400. In general, 14 day aged Z inks exhibit lower ISL than their 10 day aged counterparts, whereas the printability of ZP inks is statistically similar after 10 or 14 days of maturation. As expected, the fluidity is also higher for ZP than for Z ink formulations. This observation is consistent with the lower viscosity conferred by the addition of PEG400 to the ink formulations (Figure 2B).

3.3. Influence of Printing Temperature on Zein Ink Printability. Temperature strongly influences ink viscosity; therefore, the extrusion temperature setting is another relevant parameter that determines printability. A temperature sweep was conducted to characterize the temperature dependence of the rheological properties of the Z and ZP formulations (Figure 5A). Interestingly, the effect of temperature on the viscosity is much greater for Z formulations (threefold) than for ZP formulations. In addition, the viscosity of aged inks is similarly affected by temperature as the shape of the viscosity versus temperature profile is similar in both fresh and aged inks. Remarkably, we identified an unexpected increase in the viscosity of both the Z and ZP formulations as the temperature is increased in the range of ~13 to ~30 °C. Further exploration of this rheology abnormality is outside the scope of this work and probably deserves a detailed analysis in future work.

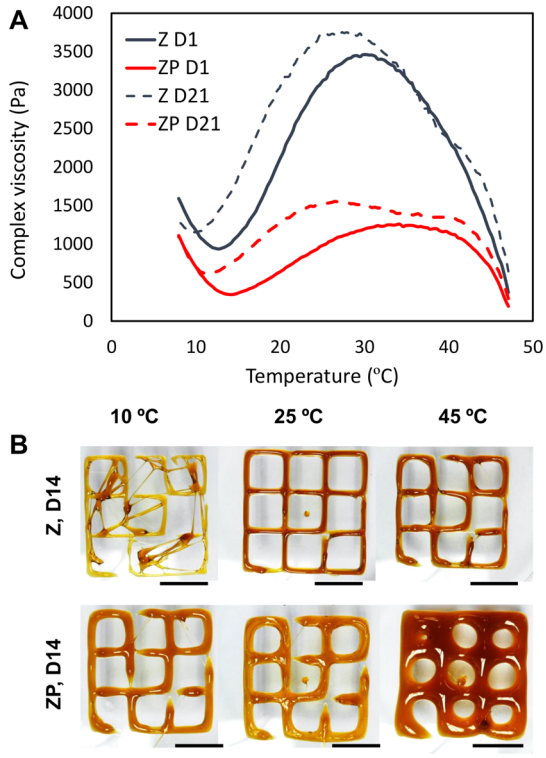

Figure 5. Temperature effect on zein ink printability. (A) Complex viscosity *vs* temperature. (B) Images of grids 3D printed at different temperatures (*i.e.*, 10, 25, and 45 °C) using Z and ZP inks 14 day old. These grids were printed at 75 kPa and 3 mm/s. Scale bar: 1 cm.

We evaluated the printability of 14 day aged Z and ZP inks at different extrusion temperatures of 10, 25, and 45 °C (see Figure 5B). The Z and ZP inks responded differently to temperature. Printability of high-viscosity inks (*i.e.*, inks with no PEG400 or aged inks) is favored at medium and high printing temperatures (25 and 45 °C), while the printability of low-viscosity inks (*i.e.*, those containing PEG400 or unaged inks) is favored by low to medium temperatures (10 and 25 °C). Extrusion of Z inks at low temperatures reveals that their increase in viscosity hinders their ability to flow and, therefore, to be successfully printed. However, the printability of younger or PEG400-containing (less viscous) inks is improved when

https://doi.org/10.1021/acsbiomaterials.1c00544
ACS Biomater. Sci. Eng. 2021, 7, 3964−3979

using low temperatures, even at 10 °C.[66] By contrast, high temperatures may be useful for printing-aged inks.

Overall, our results suggest that zein formulations may be tuned to accommodate different printing aims. By knowing the range of capacities of a particular bioprinter, one can choose an adequate formulation for a particular profile of pressures and speeds. Even for a fixed composition, the rheology of a zein-based ink can be fine-tuned by playing with different maturation times, PEG concentrations, and printing temperatures.

3.4. 3D Printing of Multilayered Constructs. We also demonstrated the capability of zein-based inks to produce multilayered 3D constructs. Figure 6A,B shows the Tecnológico de Monterrey logo and Figure 6C shows a close-up of the fine features printed using zein-based inks. The logo had a length of 13.3 cm and a height of 1.6 mm and was built using four layers of the material.

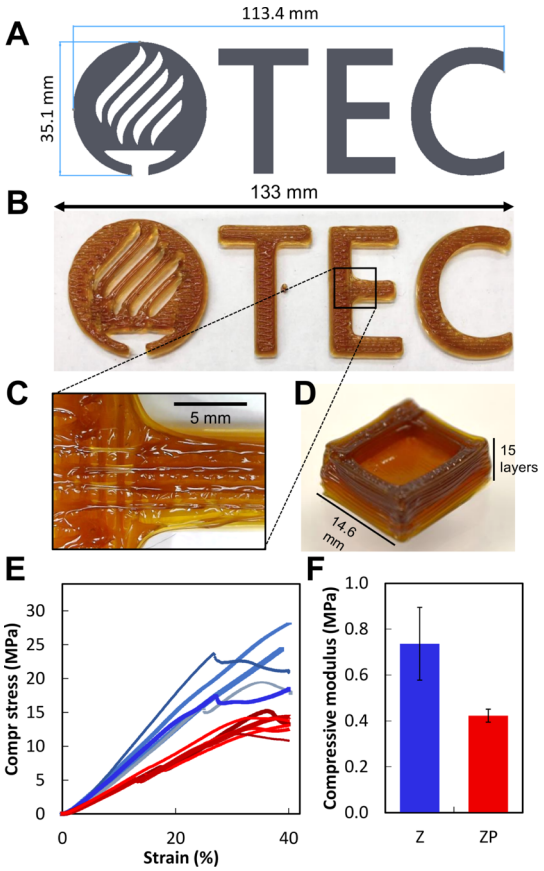

Figure 6. 3D printing of multilayered constructs. (A) "Tecnológico de Monterrey" logo in STL format. (B) 3D printed with high resolution. (C) Close-up of the logo showing the resolution of the printed structure. (D) Self-standing hollow box printed with 15 layers. The printing parameters were 85 kPa, speed 33 mm/s, and room temperature. We used a Z ink with 30 days of aging. (E) Strain *vs* stress plots derived from a compression test conducted with 3D printed cylinders of Z (blue curves; $N = 5$) and ZP (red curves; $N = 5$). (F) Young modulus of 3D printed cylinders of Z and ZP, as determined from compression tests.

We further challenged the self-standing properties of this ink by printing a hollow box (Figure 6D). The large printed constructs of more than 15 layers (6 mm) did not collapse or lose their shape. Some other publications have reported printing hollow constructs of 10−15 layers; however, the studies often used sacrificial or support materials, as well as postprinting processing.[83−85]

We studied the compressive properties of printed cylinders fabricated with Z and ZP in compressive tests. Figure 6E shows stress versus deformation curves for cylinders fabricated with Z and ZP. Several repeats of each treatment are shown to illustrate the variability of the mechanical properties among constructs. The mechanical properties of ZP constructs are more homogeneous than those of Z constructs. The addition of PEG had an important effect on the mechanical properties of the constructs. Z constructs are more elastic than ZP constructs; the Young modulus is significantly higher (approximately twofold) for Z than for ZP cylinders (Figure 6F). ZP constructs are more deformable than Z constructs. The maximum compressive strength is much higher in ZP than in Z constructs; we were able to compress ZP cylinders to more than 35% of their height before permanent deformation occurred.

3.5. Stability of Zein-Printed Constructs in Aqueous Environments. In many biological applications, such as cell culture or drug release, printed constructs will be exposed to aqueous environments for long durations.[86] Therefore, the stability of the zein-printed constructs is a relevant property for assessment. In this section, we report the response of zein constructs to aqueous environments in terms of integrity and topographical changes.

We first assessed the integrity of our printed constructs throughout typical cell culture protocols by immersing the 3D printed zein grids in cell culture medium and incubating for 7 days at 37 °C. The average thickness of the lines of the grids and their projected surface was monitored over the 7 days (Figure 7A). The ZP grids exhibited a (nonsignificant) higher stability than Z grids after 7 days of culture, but both the Z and the ZP formulations were able to withstand typical cell culture conditions. For instance, the projected surface of ZP grids, as determined by image analysis of optical micrographs, was preserved by 96.2 ± 3.35%.

Similarly, 92.40 ± 8.04% of the grid structure remained in the 3D printed Z-grids after 7 days of culture. These results suggest that the extent of erosion was moderate (3.77 and 7.59% for ZP and Z, respectively) after 1 week under culture conditions, providing evidence for stability under typical culture conditions.

Zein-based materials are known to change their surface structure upon contact with aqueous solutions due to the rearrangement of their hydrophilic and hydrophobic protein domains.[87] Exposure to water can induce changes in the secondary structure of zein chains because the ethanol used as the solvent for ink formulation is displaced by water and the hydrophilic domains of zein are forced outward.[88,89] These changes in the secondary structure were evaluated by FTIR analysis (Figure 7B), which revealed a clear difference between dry and wet samples of zein-based inks. The dry samples have a symmetrical amide I band located around 1650 cm^{-1}, while this band is skewed toward 1640 cm^{-1} in the wet zein.

We qualitatively investigated the changes in appearance of 3D printed zein constructs following exposure to water. We explored two scenarios: wetting immediately after printing and wetting after 48 h of drying in a desiccator. The process of water contact causes marked topographic changes in the surface of freshly printed zein constructs (Figure 7C). Swelling causes distinctive wrinkles on the surface of zein printings

https://doi.org/10.1021/acsbiomaterials.1c00544
ACS Biomater. Sci. Eng. 2021, 7, 3964−3979

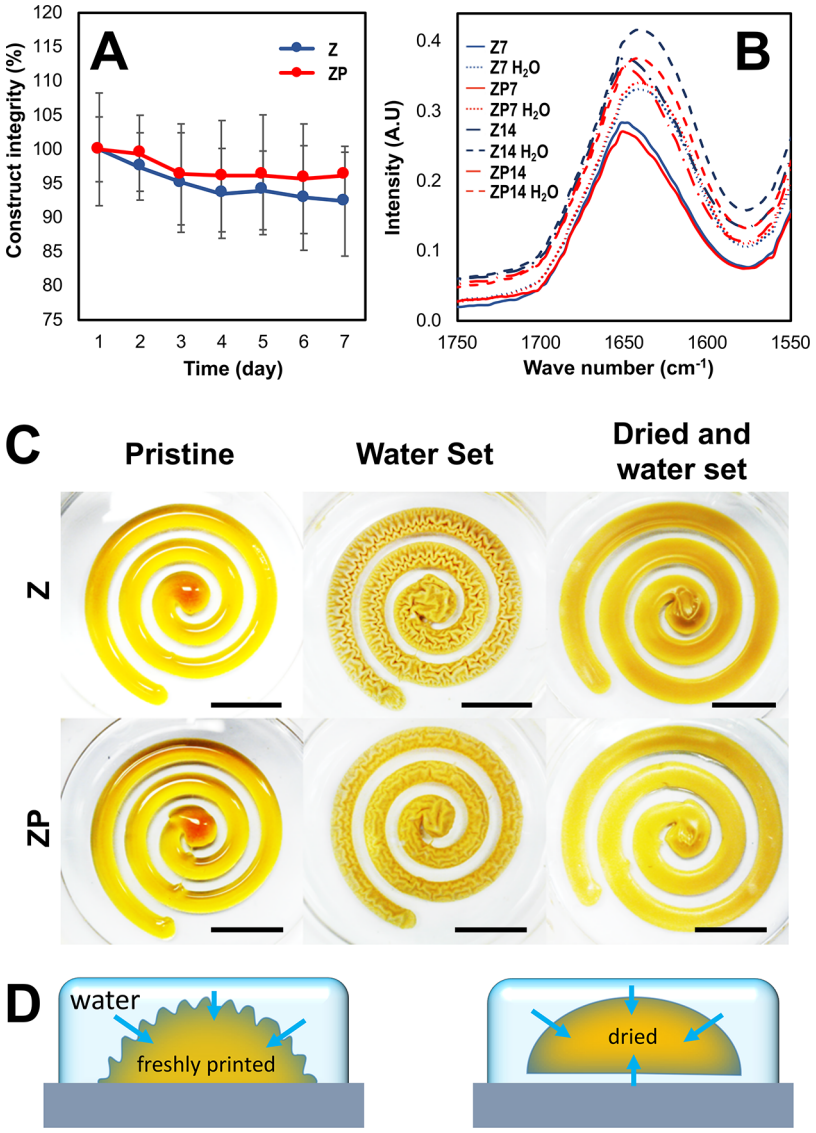

Figure 7. Stability of zein-printed constructs in aqueous environments. (A) Z and ZP construct integrity under aqueous conditions over time. (B) FTIR analysis of Z and ZP inks at two different aging times (days 7 [Z7, ZP7] and 14 [Z14, ZP14]) and after immersion in water. FTIR of samples after water immersion is indicated with the suffix H_2O. (C) Effect of wetting freshly printed or desiccated zein constructs on their surface topography. (D) Schematic representation of the effect of swelling in zein constructs.

(Video S3). Interestingly, the wrinkles are much less pronounced in ZP printings. The wrinkling effect most likely happens due to heterogeneous swelling.[87]

As schematically shown in Figure 7D, the portion of the construct directly exposed to the aqueous environment absorbs water at a faster rate than the one that is adhered to the surface. Extrusion of zein directly into water, which equally exposes all surfaces, does not lead to wrinkling. If 3D printed zein constructs are first desiccated for 48 h, thereby detached from the surface, and later immersed in water, wrinkle formation is prevented (Figure 7C,D). The wrinkles could have an undesired effect on the shape of printed zein constructs; however, they may be convenient for some applications. For instance, wrinkling might be exploited to increase surface/volume ratios. For example, we could envision applications where the addition of water greatly enhances the surface area available for cell attachment, particle adhesion, drug release, or mass transport enhancement at the surface. On the contrary, desiccation after printing reinforces the stability and fidelity of zein-printed structures and therefore their use in a wide range of biomedical applications where constructs are typically exposed to aqueous environments.

3.6. Biomedical Applications: Drug Release. Zein-based materials have been used as vehicles in pharmaceutical formulations.[48,90] For instance, zein microspheres[91] and bionanocomposites[92] have been used for drug delivery. As mentioned before, zein is classified as a safe excipient by the FDA.[93,94]

Here, we explored the feasibility of using zein inks for 3D printing of tablets containing a pharmaceutical compound to show that ink-based tablets may be effective alternatives for drug release applications and personalized therapies. We used the NA antibiotic as a pharmaceutical model in our controlled release experiments from zein-printed tablets, as NA is a first-generation quinolone-based compound that is able to mitigate narrow spectrum implant-related infections.[94−96] Figure 8A shows results of a 48 h drug-release experiment from zein-based printed tablets containing NA. A burst effect was

https://doi.org/10.1021/acsbiomaterials.1c00544
ACS Biomater. Sci. Eng. 2021, 7, 3964−3979

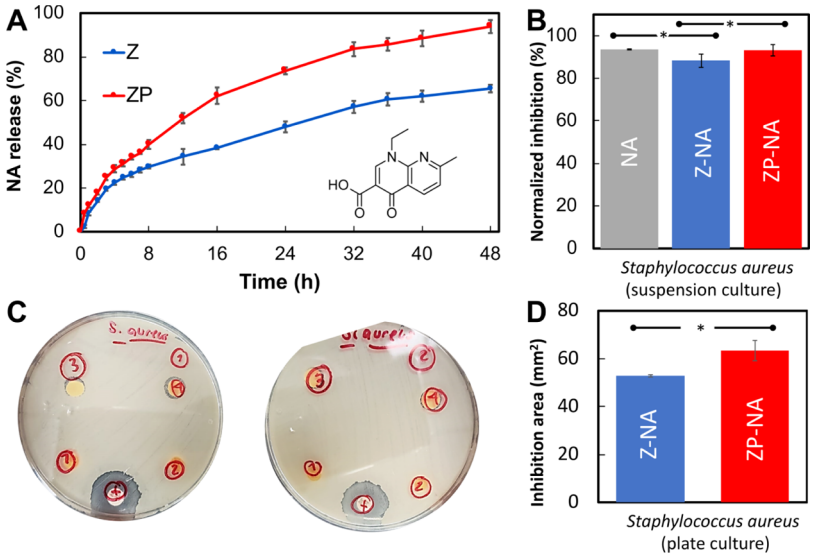

Figure 8. Drug release. (A) Cumulative release of NA from Z (blue line) and ZP (red line) for 48 h (chemical structure of NA is shown on the bottom right). (B) Bacterial inhibition by 3D printed tablets of Z-NA and ZP-NA against suspension cultures of *S. aureus*. (C,D) Bacterial inhibition caused by 3D printed tablets of Z-NA and ZP-NA against suspension cultures of *S. aureus* in plate cultures. (C) Images of two independent replicas are presented. The imbibition halos induced by a disc of NA (as a positive control) (+), 3D printed tablets of Z-NA (1, 2), and ZP-NA (3, 4) are shown, and (D) their area was quantified by image analysis.

observed for Z and ZP during the first 8 h, with a release of 29.83 ± 0.87 and 39.90 ± 2.04% of the drug, respectively. The incorporation of PEG400 enhanced the burst effect by 10%, arguably because zein chains are less entangled and allow faster diffusion of the NA through the polymeric matrix. The hydrophilicity of PEG400 may also play an important role in the diffusion of NA, as shown elsewhere for different pharmaceutics and drug-delivery materials.[97,98] At 48 h, a significantly higher NA load was released from the ZP tablet formulations (93.84 ± 2.98%) than from the Z formulations (65.49 ± 1.73%).

We also determined the antibacterial activity of 3D printed zein tablets formulated with NA against suspension cultures of *S. aureus* (Figure 8B). Four different tablet compositions (pristine Z, pristine ZP, Z with added NA [Z-NA], and ZP with added NA [ZP-NA]) were evaluated. Control experiments with direct NA application (without zein) showed that the NA drastically inhibits the growth of *S. aureus* at the concentrations tested. We observed a decrease of 93.60% in the absorbance of *S. aureus* suspension cultures, which is in agreement with previous reports.[99,100]

We also evaluated the antibacterial effect of 3D printed Z and ZP tablets containing a controlled-release dose of 3 mg NA per g of zein. We observed a decrease of 88.27% in absorbance of the bacterial culture after 48 h in experiments where Z-NA 3D printed tablets were added to *S. aureus* suspension cultures (Figure 8B) and plate cultures (Figure 8C,D). The antibacterial activity was higher for the ZP-NA tablets, which caused a 93.20% decrease in the absorbance of *S. aureus* suspension cultures. ZP-NA 3D printed tablets also induced significantly larger inhibition halos than Z-NA tablets in solid agar cultures 48 h after plating highly concentrated *S. aureus* suspensions (10^7 cells mL^{-1}).

3.7. Biomedical Applications: Cellular Scaffolding. We also explored the feasibility of using 3D printed zein scaffolds to support cell cultures. For this purpose, 2 × 2 cm grids were printed, desiccated, UV-sterilized, and washed with PBS 3 times to remove any residual ethanol. High residual concentrations of ethanol in the zein-based scaffolds may inhibit cell proliferation. We therefore conducted FTIR determinations of the ethanol present in samples of the PBS used for washing of the zein scaffolds prior to cell culture. None of washing supernatants from Z and ZP samples showed an EtOH-related peak in our FTIR analysis. Since the limit of detection of ethanol peaks in the FTIR spectrum was 1.25% EtOH in PBS, we can conclude that the ethanol concentration in the washing supernatant is equal to or smaller than 1.25%. However, we expect the concentration to be close to 0 after 7 days of desiccation, UV sterilization, and PBS washing and we do not anticipate interference from EtOH during cell culture. The resulting PBS-swollen scaffolds showed a smooth surface similar to that of the dried/water set spirals shown in Figure 7C. We evaluated cell attachment and morphology using optical and fluorescence microscopy (Figure 9A,B) and we determined cell viability over time using the PrestoBlue assay in C2C12 cells cultured on these zein surfaces (Figure 9C). We observed that cell attachment and spreading was not favored on untreated 3D printed Z and ZP surfaces.

For instance, Figure 9A shows only limited cell attachment on Z-printed constructs, as revealed by the tendency to form agglomerates of cells (colonies) instead of a homogeneous monolayer on the surface. Note, however, that the formation of cell agglomerates anchored to Z constructs could be useful in organ-on-chip scenarios; that is, to conduct anticancer drug screening using anchored 3D cell aggregates (*i.e.*, tumoroids). Figure 9B also shows very low cell attachment to ZP-printed constructs. The metabolic activity of C2C12 cells was higher when cultured on 3D printed Z grids than on ZP grids (Figure 9A–C). Taken together with the metabolic activity data, the microscopy examination indicates that zein-based materials are cytocompatible but provide limited anchorage capacity (zein does not exhibit cell anchorage sequences, such as RGD) for cell attachment.

We conducted an additional set of cell culture experiments using 3D printed zein-based grids coated with fibronectin, a widely used cell-adhesive protein.[101] We then compared actin/

https://doi.org/10.1021/acsbiomaterials.1c00544
ACS Biomater. Sci. Eng. 2021, 7, 3964–3979

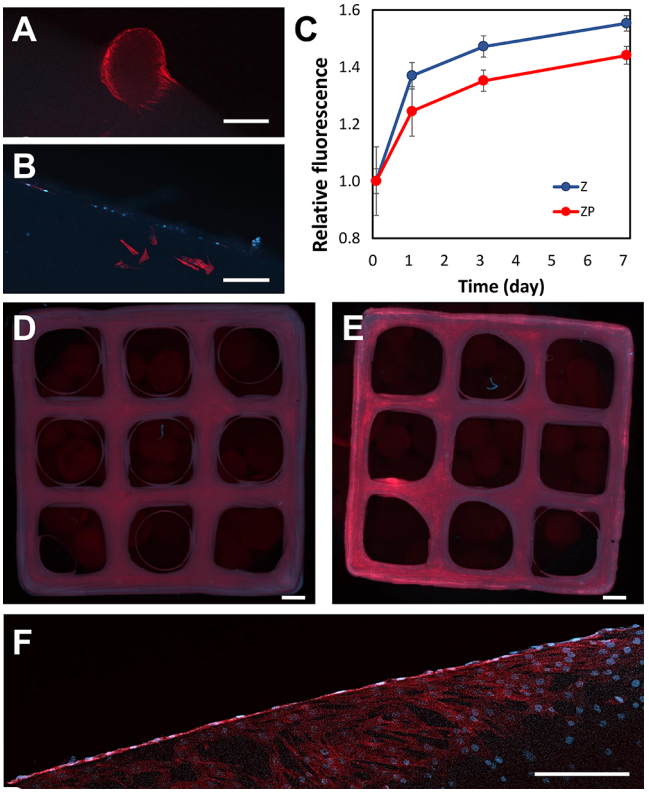

Figure 9. Zein-based 3D printed constructs as cellular scaffolds. (A) Actin (red)-stained C2C12 agglomerate formed on the surface of a grid printed with Z at day 3 of culture; scale bar: 200 μm. (B) Actin (red)/nucleic (blue)/staining of C2C12 cells at day 7 of culture on a ZP grid; scale bar: 200 μm. (C) Normalized C2C12 myoblast PrestoBlue proliferation assay on the 3D printed grids of Z (blue) and ZP (red) over 7 days of culture. (D) Actin (red)/nucleic (blue) staining of C2C12 cells at day 7 of culture on a ZP grid; scale bar: 2000 μm. (E) Actin (red)/nucleic (blue) staining of C2C12 cells at day 7 of culture on ZP grids covered with fibronectin; scale bar: 2000 μm. (F) Closeup of cells spreading at day 7 of culture on ZP grids covered with fibronectin, scale bar: 200 μm.

nucleic fluorescent staining on grids of ZP (Figure 9D) and ZP with fibronectin (Figure 9E) after 7 days of C2C12 cell culture. The close-up micrographs of the ZP with fibronectin grids (Figure 9F) showed that the fibronectin coating significantly enhanced cell attachment and spreading. Overall, these results provide evidence of the potential use of 3D-printed zein-based materials as cell culture substrates. Zein differs from other biopolymers because it is a hydrophobic protein. This characteristic makes it stable under aqueous conditions (without the need for any chemical modification). In addition, unlike most biopolymers used for 3D printing, zein does not require a cross-linking agent during the printing process. Fibronectin coating is simple, low-cost, and widely used; therefore, this coating step does not represent a major drawback for the use of zein in cell culture applications.

4. CONCLUSIONS

The current portfolio of 3D printable proteins is limited. Here, we introduced and characterized 3D printing inks based on zein, which is the main constitutive protein in maize seeds and a highly available and low-cost material. These inks are easily prepared with standard laboratory tools and their rheology, and thus printability, can be tuned by altering the aging time and/or printing temperature or by the addition of plasticizers such as PEG. Printability was analyzed for three different printing pressures and three different printhead velocities. These parameters can be adjusted to achieve a desired printing resolution depending on the different rheological properties of the inks. Remarkably, unlike other protein-based inks, our zein inks generated 3D printed structures with no requirement for either a prechemical functionalization or a poststabilizing process. These inks are therefore highly versatile for use in 3D printing applications.

Knowing the range of capacities of a particular bioprinter, one can choose an adequate formulation for a particular profile of pressures and speeds. Even for a fixed composition, one can tune the rheology of a zein-based ink by manipulating the maturation times and the printing temperature. Proof-of-concept studies confirmed that printed zein constructs can be used for drug-release applications. We also explored the use of zein inks in the fabrication of 3D printed cell scaffolds. Zein-based grids were coated with fibronectin and seeded with myoblasts. We observed successful cell attachment, spreading, and viability over a period of 7 days.

These inks are easily prepared with standard laboratory tools. In addition, their rheology, and therefore their printability, can be tuned by altering the aging time and/or printing temperature or by the addition of plasticizers such as PEG. However, attention should be paid to the fact that zein is a natural polymer that may vary from batch to batch.[102] Additional tunings may be needed to match the printability of zein-based inks formulated using different zein batches. We anticipate that 3D printing with zein based inks will open the door to versatile applications in diverse fields and especially biomedical applications.

■ ASSOCIATED CONTENT

Supporting Information

The Supporting Information is available free of charge at https://pubs.acs.org/doi/10.1021/acsbiomaterials.1c00544.

Data related to a complementary characterization of zein-based inks (Z and ZP inks) and the constructs printed using these inks, including FTIR analysis of the zein-based inks that shows the effect of aging time and water interaction in the secondary structure of the protein, analysis of the microstructure, at the cross-section of zein constructs, as observed using SEM, experimental data, derived from a rheological characterization, and ISL values and their corresponding standard deviations (PDF)

Video 1 shows experiments in which multilayered constructs are 3D printed using zein-based inks (MOV)

Video 2 shows experiments in which multilayered constructs are 3D printed using zein-based inks (MOV)

Video 3 shows the wrinkling effect that zein-based inks exhibit when exposed to water while adhered to a solid surface. The exposed surface absorbs water faster than the unexposed surface and asymmetrically swelling causes characteristic wrinkles (MOV)

https://doi.org/10.1021/acsbiomaterials.1c00544
ACS Biomater. Sci. Eng. 2021, 7, 3964−3979

AUTHOR INFORMATION

Corresponding Authors

Mario Moisés Alvarez − *Centro de Biotecnología-FEMSA and Departamento de Bioingeniería, Escuela de Ingeniería y Ciencias, Tecnologico de Monterrey, Monterrey 64849, Nuevo León, Mexico*; Email: mario.alvarez@tec.mx

Grissel Trujillo-de Santiago − *Centro de Biotecnología-FEMSA and Departamento de Ingeniería Mecatrónica y Eléctrica, Escuela de Ingeniería y Ciencias, Tecnologico de Monterrey, Monterrey 64849, Nuevo León, Mexico*; orcid.org/0000-0001-9230-4607; Email: grissel@tec.mx

Authors

Jorge Alfonso Tavares-Negrete − *Centro de Biotecnología-FEMSA and Departamento de Bioingeniería, Escuela de Ingeniería y Ciencias, Tecnologico de Monterrey, Monterrey 64849, Nuevo León, Mexico*; orcid.org/0000-0001-7695-460X

Alberto Emanuel Aceves-Colin − *Centro de Biotecnología-FEMSA and Departamento de Ingeniería Mecatrónica y Eléctrica, Escuela de Ingeniería y Ciencias, Tecnologico de Monterrey, Monterrey 64849, Nuevo León, Mexico*

Delia Cristal Rivera-Flores − *Centro de Biotecnología-FEMSA and Departamento de Ciencias, Escuela de Ingeniería y Ciencias, Tecnologico de Monterrey, Monterrey 64849, Nuevo León, Mexico*

Gladys Guadalupe Díaz-Armas − *Centro de Biotecnología-FEMSA and Departamento de Ingeniería Mecatrónica y Eléctrica, Escuela de Ingeniería y Ciencias, Tecnologico de Monterrey, Monterrey 64849, Nuevo León, Mexico*

Anne-Sophie Mertgen − *Centro de Biotecnología-FEMSA and Departamento de Bioingeniería, Escuela de Ingeniería y Ciencias, Tecnologico de Monterrey, Monterrey 64849, Nuevo León, Mexico*

Plinio Alejandro Trinidad-Calderón − *Centro de Biotecnología-FEMSA and Departamento de Bioingeniería, Escuela de Ingeniería y Ciencias, Tecnologico de Monterrey, Monterrey 64849, Nuevo León, Mexico*; orcid.org/0000-0002-5930-1997

Jorge Miguel Olmos-Cordero − *Centro de Biotecnología-FEMSA and Departamento de Ingeniería Mecatrónica y Eléctrica, Escuela de Ingeniería y Ciencias, Tecnologico de Monterrey, Monterrey 64849, Nuevo León, Mexico*

Elda Graciela Gómez-López − *Departamento de Ciencias, Escuela de Ingeniería y Ciencias, Tecnologico de Monterrey, Monterrey 64849, Nuevo León, Mexico*

Esther Pérez-Carrillo − *Centro de Biotecnología-FEMSA and Departamento de Bioingeniería, Escuela de Ingeniería y Ciencias, Tecnologico de Monterrey, Monterrey 64849, Nuevo León, Mexico*; orcid.org/0000-0003-2636-6281

Zamantha Judith Escobedo-Avellaneda − *Centro de Biotecnología-FEMSA and Departamento de Bioingeniería, Escuela de Ingeniería y Ciencias, Tecnologico de Monterrey, Monterrey 64849, Nuevo León, Mexico*

Ali Tamayol − *Department of Biomedical Engineering, University of Connecticut Health Center, Farmington, Connecticut 06030, United States*; orcid.org/0000-0003-1801-2889

Complete contact information is available at: https://pubs.acs.org/10.1021/acsbiomaterials.1c00544

Author Contributions

#J.A.T.-N. and A.E.A.-C. contributed equally. D.C.R.-F., G.G.D.-A., and A.-S.M. contributed equally.

Funding

J.A.T.-N., P.A.T.-C., and J.M.O.-C. gratefully acknowledge the financial support received from CONACyT (Consejo Nacional de Ciencia y Tecnología, México) in the form of Graduate Program Scholarships. A.-S.M., M.M.A., and G.T.-d.S. acknowledge the institutional funding received from Tecnológico de Monterrey (grant 002EICIS01). M.M.A. and G.T.-d.S. acknowledge funding provided by CONACyT (Consejo Nacional de Ciencia y Tecnología, México) through grants SNI 26048 and SNI 256730, respectively. M.M.A. and G.T.-d.S. acknowledge the support of the CELLINK partnership program. M.M.A. and G.T.-d.S. acknowledge the support of Zapote Negro in the form of meal sponsorship for students at the Alvarez-Trujillo Laboratory. G.T.-d.S. acknowledges the funding received from L'Oréal-UNESCO-CONACyT-AMC (National Fellowship for Women in Science, Mexico). A.T. would like to acknowledge the financial support of the National Institutes of Health (GM126831 and AR073822).

Notes

The authors declare no competing financial interest.

REFERENCES

(1) Sánchez-Salazar, M. G.; Álvarez, M. M.; Trujillo-de Santiago, G. Advances in 3D Bioprinting for the Biofabrication of Tumor Models. *Bioprinting* **2021**, *21*, No. e00120.

(2) Nagarajan, N.; Dupret-Bories, A.; Karabulut, E.; Zorlutuna, P.; Vrana, N. E. Enabling Personalized Implant and Controllable Biosystem Development through 3D Printing. *Biotechnol. Adv.* **2018**, *36*, 521−533.

(3) Sreenilayam, S. P.; Ahad, I. U.; Nicolosi, V.; Acinas Garzon, V.; Brabazon, D. Advanced Materials of Printed Wearables for Physiological Parameter Monitoring. *Mater. Today* **2020**, *32*, 147−177.

(4) Handral, H. K.; Hua Tay, S.; Wan Chan, W.; Choudhury, D. 3D Printing of Cultured Meat Products. *Crit. Rev. Food Sci. Nutr.* **2020**, 1−10.

(5) Liu, J.; Sun, L.; Xu, W.; Wang, Q.; Yu, S.; Sun, J. Current Advances and Future Perspectives of 3D Printing Natural-Derived Biopolymers. *Carbohydr. Polym.* **2019**, *207*, 297−316.

(6) Provaggi, E.; Kalaskar, D. M. 3D Printing Families: Laser, Powder, Nozzle Based Techniques. *3D Printing in Medicine*; Elsevier, 2017; pp 21−42.

(7) Gaisford, S. 3D Printed Pharmaceutical Products. *3D Printing in Medicine*; Elsevier, 2017; pp 155−166.

(8) Roopavath, U. K.; Kalaskar, D. M. Introduction to 3D Printing in Medicine. *3D Printing in Medicine*; Elsevier, 2017; pp 1−20.

(9) Skardal, A.; Devarasetty, M.; Kang, H.-W.; Mead, I.; Bishop, C.; Shupe, T.; Lee, S. J.; Jackson, J.; Yoo, J.; Soker, S.; Atala, A. A Hydrogel Bioink Toolkit for Mimicking Native Tissue Biochemical and Mechanical Properties in Bioprinted Tissue Constructs. *Acta Biomater.* **2015**, *25*, 24−34.

(10) Zhang, K.; Fu, Q.; Yoo, J.; Chen, X.; Chandra, P.; Mo, X.; Song, L.; Atala, A.; Zhao, W. 3D Bioprinting of Urethra with PCL/PLCL Blend and Dual Autologous Cells in Fibrin Hydrogel: An in Vitro Evaluation of Biomimetic Mechanical Property and Cell Growth Environment. *Acta Biomater.* **2017**, *50*, 154−164.

(11) Farzin, A.; Miri, A. K.; Sharifi, F.; Faramarzi, N.; Jaberi, A.; Mostafavi, A.; Solorzano, R.; Zhang, Y. S.; Annabi, N.; Khademhosseini, A.; Tamayol, A. 3D-Printed Sugar-Based Stents Facilitating Vascular Anastomosis. *Adv. Healthcare Mater.* **2018**, *7*, 1800702.

(12) Jovic, T. H.; Kungwengwe, G.; Mills, A. C.; Whitaker, I. S. Plant-Derived Biomaterials: A Review of 3D Bioprinting and Biomedical Applications. *Front. Mech. Eng.* **2019**, *5*, 19.
(13) Shie, M.-Y.; Shen, Y.-F.; Astuti, S. D.; Lee, A. K.-X.; Lin, S.-H.; Dwijaksara, N. L. B.; Chen, Y.-W. Review of Polymeric Materials in 4D Printing Biomedical Applications. *Polymers* **2019**, *11*, 1864.
(14) Rodríguez-Salvador, M.; Villarreal-Garza, D.; Álvarez, M. M.; Santiago, G. T. Analysis of the Knowledge Landscape of Three-Dimensional Bioprinting in Latin America. *Int. J. Bioprint.* **2019**, *5*, 240.
(15) Hölzl, K.; Lin, S.; Tytgat, L.; Van Vlierberghe, S.; Gu, L.; Ovsianikov, A. Bioink Properties before, during and after 3D Bioprinting. *Biofabrication* **2016**, *8*, 032002.
(16) Kyle, S.; Jessop, Z. M.; Al-Sabah, A.; Whitaker, I. S. 'Printability' of Candidate Biomaterials for Extrusion Based 3D Printing: State-of-the-Art. *Adv. Healthcare Mater.* **2017**, *6*, 1700264.
(17) Rodríguez-Salvador, M.; Villarreal-Garza, D.; Álvarez, M. M.; Santiago, G. T. de. Analysis of the Knowledge Landscape of Three-Dimensional Bioprinting in Latin America. *Int. J. Bioprint.* **2019**, *5*, 240.
(18) Godoi, F. C.; Prakash, S.; Bhandari, B. R. 3d Printing Technologies Applied for Food Design: Status and Prospects. *J. Food Eng.* **2016**, *179*, 44−54.
(19) Dankar, I.; Haddarah, A.; Omar, F. E. L.; Sepulcre, F.; Pujolà, M. 3D Printing Technology: The New Era for Food Customization and Elaboration. *Trends Food Sci. Technol.* **2018**, *75*, 231−242.
(20) Yang, F.; Zhang, M.; Prakash, S.; Liu, Y. Physical Properties of 3D Printed Baking Dough as Affected by Different Compositions. *Innovative Food Sci. Emerging Technol.* **2018**, *49*, 202−210.
(21) Bégin-Drolet, A.; Dussault, M.-A.; Fernandez, S. A.; Larose-Dutil, J.; Leask, R. L.; Hoesli, C. A.; Ruel, J. Design of a 3D Printer Head for Additive Manufacturing of Sugar Glass for Tissue Engineering Applications. *Addit. Manuf.* **2017**, *15*, 29−39.
(22) Liu, Z.; Bhandari, B.; Zhang, M. Incorporation of Probiotics (Bifidobacterium Animalis Subsp. Lactis) into 3D Printed Mashed Potatoes: Effects of Variables on the Viability. *Food Res. Int.* **2020**, *128*, 108795.
(23) Yang, J.; An, X.; Liu, L.; Tang, S.; Cao, H.; Xu, Q.; Liu, H. Cellulose, Hemicellulose, Lignin, and Their Derivatives as Multi-Components of Bio-Based Feedstocks for 3D Printing. *Carbohydr. Polym.* **2020**, *250*, 116881.
(24) Lee, J. G.; Guo, Y.; Belgodere, J. A.; Al Harraq, A.; Hymel, A. A.; Pete, A. J.; Valsaraj, K. T.; Benton, M. G.; Miller, M. G.; Jung, J. P.; Bharti, B. Lignin-Zein Composite: Synthesis, Three-Dimensional Printing, and Microbial Degradation. *ACS Sustainable Chem. Eng.* **2021**, *9*, 1781−1789.
(25) Teng, X.; Zhang, M.; Bhandri, B. 3D Printing of *Cordyceps* Flower Powder. *J. Food Process Eng.* **2019**, *42*, No. e13179.
(26) An, Y.-J.; Guo, C.-F.; Zhang, M.; Zhong, Z.-P. Investigation on Characteristics of 3D Printing Using *Nostoc Sphaeroides* Biomass. *J. Sci. Food Agric.* **2019**, *99*, 639−646.
(27) Anukiruthika, T.; Moses, J. A.; Anandharamakrishnan, C. 3D Printing of Egg Yolk and White with Rice Flour Blends. *J. Food Eng.* **2020**, *265*, 109691.
(28) Mantihal, S.; Prakash, S.; Bhandari, B. Texture-modified 3D Printed Dark Chocolate: Sensory Evaluation and Consumer Perception Study. *J. Texture Stud.* **2019**, *50*, 386−399.
(29) Lanaro, M.; Desselle, M. R.; Woodruff, M. A. 3D Printing Chocolate: Properties of Formulations for Extrusion, Sintering, Binding and Ink Jetting. *Fundamentals of 3D Food Printing and Applications*; Elsevier, 2019; pp 151−173.
(30) Lille, M.; Nurmela, A.; Nordlund, E.; Metsä-Kortelainen, S.; Sozer, N. Applicability of Protein and Fiber-Rich Food Materials in Extrusion-Based 3D Printing. *J. Food Eng.* **2018**, *220*, 20−27.
(31) Ross, M. M.; Kelly, A. L.; Crowley, S. V. Potential Applications of Dairy Products, Ingredients and Formulations in 3D Printing. *Fundamentals of 3D Food Printing and Applications*; Elsevier, 2019; pp 175−206.
(32) Dick, A.; Bhandari, B.; Prakash, S. 3D printing of meat. *Meat Sci.* **2019**, *153*, 35−44.
(33) Azzollini, D.; Derossi, A.; Fogliano, V.; Lakemond, C. M. M.; Severini, C. Effects of Formulation and Process Conditions on Microstructure, Texture and Digestibility of Extruded Insect-Riched Snacks. *Innovative Food Sci. Emerging Technol.* **2018**, *45*, 344−353.
(34) Le Tohic, C.; O'Sullivan, J. J.; Drapala, K. P.; Chartrin, V.; Chan, T.; Morrison, A. P.; Kerry, J. P.; Kelly, A. L. Effect of 3D Printing on the Structure and Textural Properties of Processed Cheese. *J. Food Eng.* **2018**, *220*, 56−64.
(35) Liu, L.; Yang, X.; Bhandari, B.; Meng, Y.; Prakash, S. Optimization of the Formulation and Properties of 3D-Printed Complex Egg White Protein Objects. *Foods* **2020**, *9*, 164.
(36) Phuhongsung, P.; Zhang, M.; Bhandari, B. 4D Printing of Products Based on Soy Protein Isolate via Microwave Heating for Flavor Development. *Food Res. Int.* **2020**, *137*, 109605.
(37) Duan, B.; Kapetanovic, E.; Hockaday, L. A.; Butcher, J. T. Three-Dimensional Printed Trileaflet Valve Conduits Using Biological Hydrogels and Human Valve Interstitial Cells. *Acta Biomater.* **2014**, *10*, 1836−1846.
(38) Sharma, R.; Smits, I. P. M.; De La Vega, L.; Lee, C.; Willerth, S. M. 3D Bioprinting Pluripotent Stem Cell Derived Neural Tissues Using a Novel Fibrin Bioink Containing Drug Releasing Microspheres. *Front. Bioeng. Biotechnol.* **2020**, *8*, 57.
(39) Kundu, J.; Pati, F.; Hun Jeong, Y.; Cho, D.-W. Biomaterials for Biofabrication of 3D Tissue Scaffolds. *Biofabrication*; Elsevier, 2013; pp 23−46.
(40) Gopinathan, J.; Noh, I. Recent Trends in Bioinks for 3D Printing. *Biomater. Res.* **2018**, *22*, 11.
(41) Ouyang, L.; Yao, R.; Zhao, Y.; Sun, W. Effect of Bioink Properties on Printability and Cell Viability for 3D Bioplotting of Embryonic Stem Cells. *Biofabrication* **2016**, *8*, 035020.
(42) Zhao, Y.; Li, Y.; Mao, S.; Sun, W.; Yao, R. The Influence of Printing Parameters on Cell Survival Rate and Printability in Microextrusion-Based 3D Cell Printing Technology. *Biofabrication* **2015**, *7*, 045002.
(43) Zhu, M.; Wang, Y.; Ferracci, G.; Zheng, J.; Cho, N.-J.; Lee, B. H. Gelatin Methacryloyl and Its Hydrogels with an Exceptional Degree of Controllability and Batch-to-Batch Consistency. *Sci. Rep.* **2019**, *9*, 6863.
(44) Kim, P.; Yuan, A.; Nam, K.-H.; Jiao, A.; Kim, D.-H. Fabrication of Poly(Ethylene Glycol): Gelatin Methacrylate Composite Nanostructures with Tunable Stiffness and Degradation for Vascular Tissue Engineering. *Biofabrication* **2014**, *6*, 024112.
(45) Yu, Y.; Guo, L.; Wang, W.; Wu, J.; Yuan, Z. Dual-Peptide-Modified Alginate Hydrogels for the Promotion of Angiogenesis. *Sci. China: Chem.* **2015**, *58*, 1866−1874.
(46) Mu, X.; Wang, Y.; Guo, C.; Li, Y.; Ling, S.; Huang, W.; Cebe, P.; Hsu, H. H.; De Ferrari, F.; Jiang, X.; Xu, Q.; Balduini, A.; Omenetto, F. G.; Kaplan, D. L. 3D Printing of Silk Protein Structures by Aqueous Solvent-Directed Molecular Assembly. *Macromol. Biosci.* **2020**, *20*, 1900191.
(47) Demir, M.; Ramos-Rivera, L.; Silva, R.; Nazhat, S. N.; Boccaccini, A. R. Zein-Based Composites in Biomedical Applications. *J. Biomed. Mater. Res., Part A* **2017**, *105*, 1656−1665.
(48) Gagliardi, A.; Froiio, F.; Salvatici, M. C.; Paolino, D.; Fresta, M.; Cosco, D. Characterization and Refinement of Zein-Based Gels. *Food Hydrocolloids* **2020**, *101*, 105555.
(49) Wang, Y.; Rakotonirainy, A. M.; Padua, G. W. Thermal Behavior of Zein-Based Biodegradable Films. *Starch/Staerke* **2003**, *55*, 25−29.
(50) Sun, Q.-S.; Dong, J.; Lin, Z.-X.; Yang, B.; Wang, J.-Y. Comparison of Cytocompatibility of Zein Film with Other Biomaterials and Its Degradability in Vitro. *Biopolymers* **2005**, *78*, 268−274.
(51) Corradini, E.; Curti, P.; Meniqueti, A.; Martins, A.; Rubira, A.; Muniz, E. Recent Advances in Food-Packing, Pharmaceutical and Biomedical Applications of Zein and Zein-Based Materials. *Int. J. Mol. Sci.* **2014**, *15*, 22438−22470.

https://doi.org/10.1021/acsbiomaterials.1c00544
ACS Biomater. Sci. Eng. 2021, 7, 3964−3979

(52) Kariduraganavar, M. Y.; Heggannavar, G. B.; Amado, S.; Mitchell, G. R. Protein Nanocarriers for Targeted Drug Delivery for Cancer Therapy. *Nanocarriers for Drug Delivery*; Elsevier Inc., 2019.
(53) Trujillo-de Santiago, G.; Portales-Cabrera, C. G.; Portillo-Lara, R.; Araiz-Hernández, D.; Del Barone, M. C.; García-López, E.; Rojas-de Gante, C.; de los Angeles De Santiago-Miramontes, M.; Segoviano-Ramírez, J. C.; García-Lara, S.; Rodríguez-González, C. Á.; Alvarez, M. M.; Di Maio, E.; Iannace, S. Supercritical CO2 Foaming of Thermoplastic Materials Derived from Maize: Proof-of-Concept Use in Mammalian Cell Culture Applications. *PLoS One* **2015**, *10*, No. e0122489.
(54) Chen, S.; Han, Y.; Huang, J.; Dai, L.; Du, J.; McClements, D. J.; Mao, L.; Liu, J.; Gao, Y. Fabrication and Characterization of Layer-by-Layer Composite Nanoparticles Based on Zein and Hyaluronic Acid for Codelivery of Curcumin and Quercetagetin. *ACS Appl. Mater. Interfaces* **2019**, *11*, 16922−16933.
(55) Mascia, L.; Zhang, W.; Gatto, F.; Scarpellini, A.; Pompa, P. P.; Mele, E. In Situ Generation of ZnO Nanoparticles within a Polyethyleneimine Matrix for Antibacterial Zein Fibers. *ACS Appl. Polym. Mater.* **2019**, *1*, 1707−1716.
(56) Kimna, C.; Tamburaci, S.; Tihminlioglu, F. Novel Zein-based Multilayer Wound Dressing Membranes with Controlled Release of Gentamicin. *J. Biomed. Mater. Res., Part B* **2019**, *107*, 2057−2070.
(57) Jing, L.; Wang, X.; Liu, H.; Lu, Y.; Bian, J.; Sun, J.; Huang, D. Zein Increases the Cytoaffinity and Biodegradability of Scaffolds 3D-Printed with Zein and Poly(ε-Caprolactone) Composite Ink. *ACS Appl. Mater. Interfaces* **2018**, *10*, 18551−18559.
(58) Jing, L.; Sun, J.; Liu, H.; Wang, X.; Huang, D. Using Plant Proteins to Develop Composite Scaffolds for Cell Culture Applications. *Int. J. Bioprint.* **2021**, *7*, 66−77.
(59) Shi, C.; Xi, S.; Han, Y.; Zhang, H.; Liu, J.; Li, Y. Structure, Rheology and Electrospinning of Zein and Poly(Ethylene Oxide) in Aqueous Ethanol Solutions. *Chin. Chem. Lett.* **2019**, *30*, 305−310.
(60) Lawton, J. W. Zein: A History of Processing and Use. *Cereal Chem.* **2002**, *79*, 1−18.
(61) Yang, H.; Yang, S.; Kong, J.; Dong, A.; Yu, S. Obtaining Information about Protein Secondary Structures in Aqueous Solution Using Fourier Transform IR Spectroscopy. *Nat. Protoc.* **2015**, *10*, 382−396.
(62) Melvin, J. A.; Lashua, L. P.; Kiedrowski, M. R.; Yang, G.; Deslouches, B.; Montelaro, R. C.; Bomberger, J. M. Simultaneous Antibiofilm and Antiviral Activities of an Engineered Antimicrobial Peptide during Virus-Bacterium Coinfection. *mSphere* **2016**, *1*, e00083−16.
(63) Chaudhari, A. A.; Joshi, S.; Vig, K.; Sahu, R.; Dixit, S.; Baganizi, R.; Dennis, V. A.; Singh, S. R.; Pillai, S. A Three-Dimensional Human Skin Model to Evaluate the Inhibition of Staphylococcus Aureus by Antimicrobial Peptide-Functionalized Silver Carbon Nanotubes. *J. Biomater. Appl.* **2019**, *33*, 924−934.
(64) CLSI. *Performance Standards for Antimicrobial Susceptibility Testing*, 29th ed.; Clinical and Laboratory Standards Institute: Wayne, PA, 2019.
(65) Di Maio, E.; Mali, R.; Iannace, S. Investigation of Thermoplasticity of Zein and Kafirin Proteins: Mixing Process and Mechanical Properties. *J. Polym. Environ.* **2010**, *18*, 626−633.
(66) Trujillo-de Santiago, G.; Rojas-de Gante, C.; García-Lara, S.; Verdolotti, L.; Di Maio, E.; Iannace, S. Strategies to Produce Thermoplastic Starch−Zein Blends: Effect on Compatibilization. *J. Polym. Environ.* **2014**, *22*, 508−524.
(67) O'Connell, C.; Ren, J.; Pope, L.; Li, Y.; Mohandas, A.; Blanchard, R.; Duchi, S.; Onofrillo, C. Characterizing Bioinks for Extrusion Bioprinting: Printability and Rheology. *3D Bioprinting*; Springer, 2020; pp 111−133.
(68) Kiyotake, E. A.; Douglas, A. W.; Thomas, E. E.; Nimmo, S. L.; Detamore, M. S. Development and Quantitative Characterization of the Precursor Rheology of Hyaluronic Acid Hydrogels for Bioprinting. *Acta Biomater.* **2019**, *95*, 176−187.
(69) Paxton, N.; Smolan, W.; Böck, T.; Melchels, F.; Groll, J.; Jungst, T. Proposal to Assess Printability of Bioinks for Extrusion-Based Bioprinting and Evaluation of Rheological Properties Governing Bioprintability. *Biofabrication* **2017**, *9*, 044107.
(70) DeSimone, E.; Schacht, K.; Jungst, T.; Groll, J.; Scheibel, T. Biofabrication of 3D Constructs: Fabrication Technologies and Spider Silk Proteins as Bioinks. *Pure Appl. Chem.* **2015**, *87*, 737−749.
(71) Zheng, Z.; Wu, J.; Liu, M.; Wang, H.; Li, C.; Rodriguez, M. J.; Li, G.; Wang, X.; Kaplan, D. L. 3D Bioprinting of Self-Standing Silk-Based Bioink. *Adv. Healthcare Mater.* **2018**, *7*, 1701026.
(72) Murphy, S. V.; Atala, A. 3D Bioprinting of Tissues and Organs. *Nat. Biotechnol.* **2014**, *32*, 773−785.
(73) Sun, Y.; Liu, Z.; Zhang, L.; Wang, X.; Li, L. Effects of Plasticizer Type and Concentration on Rheological, Physico-Mechanical and Structural Properties of Chitosan/Zein Film. *Int. J. Biol. Macromol.* **2020**, *143*, 334−340.
(74) Schwab, A.; Levato, R.; D'Este, M.; Piluso, S.; Eglin, D.; Malda, J. Printability and Shape Fidelity of Bioinks in 3D Bioprinting. *Chem. Rev.* **2020**, *120*, 11028−11055.
(75) M'Barki, A.; Bocquet, L.; Stevenson, A. Linking Rheology and Printability for Dense and Strong Ceramics by Direct Ink Writing. *Sci. Rep.* **2017**, *7*, 6017.
(76) Uzun, S.; Ilavsky, J.; Padua, G. W. Characterization of Zein Assemblies by Ultra-Small-Angle X-Ray Scattering. *Soft Matter* **2017**, *13*, 3053−3060.
(77) Matsushima, N.; Danno, G.-i.; Takezawa, H.; Izumi, Y. Three-Dimensional Structure of Maize α-Zein Proteins Studied by Small-Angle X-Ray Scattering. *Biochim. Biophys. Acta, Protein Struct. Mol. Enzymol.* **1997**, *1339*, 14−22.
(78) Dong, S.; Gao, A.; Zhao, Y.; Li, Y.-t.; Chen, Y. Characterization of Physicochemical and Structural Properties of Atmospheric Cold Plasma (ACP) Modified Zein. *Food Bioprod. Process.* **2017**, *106*, 65−74.
(79) Yin, J.; Zhao, D.; Liu, J. Trends on Physical Understanding of Bioink Printability. *Bio-Des. Manuf.* **2019**, *2*, 50−54.
(80) Yuk, H.; Zhao, X. A New 3D Printing Strategy by Harnessing Deformation, Instability, and Fracture of Viscoelastic Inks. *Adv. Mater.* **2018**, *30*, 1704028.
(81) Karyappa, R.; Ching, T.; Hashimoto, M. Embedded Ink Writing (EIW) of Polysiloxane Inks. *ACS Appl. Mater. Interfaces* **2020**, *12*, 23565−23575.
(82) Guo, H. X.; Heinämäki, J.; Yliruusi, J. Stable Aqueous Film Coating Dispersion of Zein. *J. Colloid Interface Sci.* **2008**, *322*, 478−484.
(83) Liu, W.; Zhang, Y. S.; Heinrich, M. A.; De Ferrari, F.; Jang, H. L.; Bakht, S. M.; Alvarez, M. M.; Yang, J.; Li, Y.-C.; Trujillo-de Santiago, G.; Miri, A. K.; Zhu, K.; Khoshakhlagh, P.; Prakash, G.; Cheng, H.; Guan, X.; Zhong, Z.; Ju, J.; Zhu, G. H.; Jin, X.; Shin, S. R.; Dokmeci, M. R.; Khademhosseini, A. Rapid Continuous Multimaterial Extrusion Bioprinting. *Adv. Mater.* **2017**, *29*, 1604630.
(84) Liu, W.; Heinrich, M. A.; Zhou, Y.; Akpek, A.; Hu, N.; Liu, X.; Guan, X.; Zhong, Z.; Jin, X.; Khademhosseini, A.; Zhang, Y. S. Extrusion Bioprinting of Shear-Thinning Gelatin Methacryloyl Bioinks. *Adv. Healthcare Mater.* **2017**, *6*, 1601451.
(85) Chimene, D.; Kaunas, R.; Gaharwar, A. K. Hydrogel Bioink Reinforcement for Additive Manufacturing: A Focused Review of Emerging Strategies. *Adv. Mater.* **2020**, *32*, 1902026.
(86) Ying, G. L.; Jiang, N.; Maharjan, S.; Yin, Y. X.; Chai, R. R.; Cao, X.; Yang, J. Z.; Miri, A. K.; Hassan, S.; Zhang, Y. S. Aqueous Two-Phase Emulsion Bioink-Enabled 3D Bioprinting of Porous Hydrogels. *Adv. Mater.* **2018**, *30*, 1805460.
(87) Paliwal, R.; Palakurthi, S. Zein in Controlled Drug Delivery and Tissue Engineering. *J. Controlled Release* **2014**, *189*, 108−122.
(88) Sabino, M. A.; Pauchard, L.; Allain, C.; Colonna, P.; Lourdin, D. Imbibition, Desiccation and Mechanical Deformations of Zein Pills in Relation to Their Porosity. *Eur. Phys. J. E* **2006**, *20*, 29−36.
(89) Madeka, H.; Kokini, J. L. Effect of Glass Transition and Cross-Linking on Rheological Properties of Zein: Development of a Preliminary State Diagram. *Cereal Chem.* **1996**, *73*, 433−438.

https://doi.org/10.1021/acsbiomaterials.1c00544
ACS Biomater. Sci. Eng. 2021, 7, 3964−3979

(90) Labib, G. Overview on Zein Protein: A Promising Pharmaceutical Excipient in Drug Delivery Systems and Tissue Engineering. *Expert Opin. Drug Delivery* **2018**, *15*, 65−75.
(91) Liu, X.; Sun, Q.; Wang, H.; Zhang, L.; Wang, J.-Y. Microspheres of Corn Protein, Zein, for an Ivermectin Drug Delivery System. *Biomaterials* **2005**, *26*, 109−115.
(92) Alcântara, A. C. S.; Aranda, P.; Darder, M.; Ruiz-Hitzky, E. Bionanocomposites Based on Alginate−Zein/Layered Double Hydroxide Materials as Drug Delivery Systems. *J. Mater. Chem.* **2010**, *20*, 9495.
(93) Lai, L. F.; Guo, H. X. Preparation of New 5-Fluorouracil-Loaded Zein Nanoparticles for Liver Targeting. *Int. J. Pharm.* **2011**, *404*, 317−323.
(94) Zhang, Y.; Cui, L.; Che, X.; Zhang, H.; Shi, N.; Li, C.; Chen, Y.; Kong, W. Zein-Based Films and Their Usage for Controlled Delivery: Origin, Classes and Current Landscape. *J. Controlled Release* **2015**, *206*, 206−219.
(95) Ahmed, M.; Kelley, S. O. Enhancing the Potency of Nalidixic Acid toward a Bacterial DNA Gyrase with Conjugated Peptides. *ACS Chem. Biol.* **2017**, *12*, 2563−2569.
(96) Pandey, A.; Aggarwal, N.; Adholeya, A.; Kochar, M. Resurrection of Nalidixic Acid: Evaluation of Water-Based Nano-formulations as Potential Nanomedicine. *Nanoscale Res. Lett.* **2018**, *13*, 298.
(97) Zhang, K.; Tang, X.; Zhang, J.; Lu, W.; Lin, X.; Zhang, Y.; Tian, B.; Yang, H.; He, H. PEG−PLGA Copolymers: Their Structure and Structure-Influenced Drug Delivery Applications. *J. Controlled Release* **2014**, *183*, 77−86.
(98) Quintero-Ortega, I. A.; Romero-Argote, F. J.; Tavares-Negrete, J. A.; Elizalde-Peña, E. A.; Carvajal García, Z. Y.; Pérez-Pérez, C. I.; Sanchez, I. C.; Luna-Bárcenas, G.; Rosillo-de la Torre, A. Synthesis and Characterization of Simple and Binary Drug Delivery Systems for Sustainable Release of Ciprofloxacin. *Int. J. Polym. Mater. Polym. Biomater.* **2019**, *68*, 751−761.
(99) Zubair, K. U.; Shah, A. H.; Fawwad, A.; Sabir, R.; Butt, A. Frequency of Urinary Tract Infection and Antibiotic Sensitivity of Uropathogens in Patients with Diabetes. *Pak. J. Med. Sci.* **2019**, *35*, 1664−1668.
(100) MacKinnon, M. C.; Pearl, D. L.; Carson, C. A.; Parmley, E. J.; McEwen, S. A. A Comparison of Modelling Options to Assess Annual Variation in Susceptibility of Generic Escherichia Coli Isolates to Ceftiofur, Ampicillin and Nalidixic Acid from Retail Chicken Meat in Canada. *Prev. Vet. Med.* **2018**, *160*, 123−135.
(101) Wu, X.; Sun, Z.; Foskett, A.; Trzeciakowski, J. P.; Meininger, G. A.; Muthuchamy, M. Cardiomyocyte Contractile Status Is Associated with Differences in Fibronectin and Integrin Interactions. *Am. J. Physiol.: Heart Circ. Physiol.* **2010**, *298*, H2071−H2081.
(102) Oliviero, M.; Di Maio, E.; Iannace, S. Effect of Molecular Structure on Film Blowing Ability of Thermoplastic Zein. *J. Appl. Polym. Sci.* **2010**, *115*, 277−287.

https://doi.org/10.1021/acsbiomaterials.1c00544
ACS Biomater. Sci. Eng. 2021, 7, 3964−3979